

Causal Characterization of Measurement and Mechanistic Anomalies

Hendrik Suhr¹ David Kaltenpoth¹ Jilles Vreeken¹

Abstract

Root cause analysis of anomalies aims to identify those features that cause the deviation from the normal process. Existing methods ignore, however, that anomalies can arise through two fundamentally different processes: measurement errors, where data was generated normally but one or more values were recorded incorrectly, and mechanism shifts, where the causal process generating the data changed. While measurement errors can often be safely corrected, mechanistic anomalies require careful consideration. We define a causal model that explicitly captures both types by treating outliers as latent interventions on latent (“true”) and observed (“measured”) variables. We show that they are identifiable, and propose a maximum likelihood estimation approach to put this to practice. Experiments show that our method matches state-of-the-art performance in root cause localization, while it additionally enables accurate classification of anomaly types, and remains robust even when the causal DAG is unknown.

1. Introduction

Real-world datasets are often noisy and contain anomalies—samples generated by processes that deviate from the norm. These anomalies can compromise model reliability, lead to biased conclusions, or misguide scientific and engineering insights. Importantly, not all anomalies are alike: some result from measurement or data collection errors, such as sensor malfunctions or misrecorded values, while others reflect genuine deviations in the underlying causal mechanisms, indicating that the process itself has changed. We call these fundamental types of anomalies *measurement anomalies* and *mechanistic anomalies*. In many applications, it is important to tell these two apart: a faulty thermometer, for example, requires a very different response than a genuine shift in temperature.

¹CISPA Helmholtz Center for Information Security. Correspondence to: Hendrik Suhr <hendrik.suhr@cispa.de>.

Preprint. February 2, 2026.

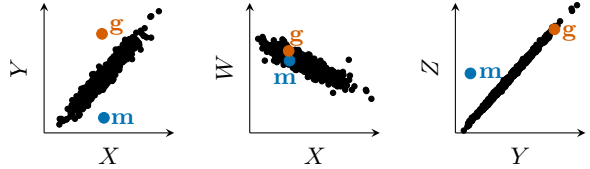


Figure 1. Different outlier types under the causal DAG $X \rightarrow Y$, $X \rightarrow W$, and $Y \rightarrow Z$. While the mechanistic outlier g only stands out when considering the $X \rightarrow Y$ relationship, the measurement outlier m stands out for $X \rightarrow Y$ and $Y \rightarrow Z$.

We give an example in Fig. 1. In the left plot, points g and m stand out. It is not immediately clear if this is due to measurement errors or changes in the mechanism that generated these points. By examining their behavior over the other causal dependencies of X and Y we can gain more insight. The middle plot, shows that neither stands out in the dependency $X \rightarrow W$. The right-hand plot, however, reveals that point m violates both $X \rightarrow Y$ and $Y \rightarrow Z$ in a way that is consistent with having measured too low a value for Y . In contrast, as the red point (g) does follow the regular relationships between $X \rightarrow W$ and $Y \rightarrow Z$, this indicates this anomaly is most likely generated by a mechanism shift between $X \rightarrow Y$.

Explainable anomaly detection (XAD) typically relies on feature-attribution methods that explain an anomaly score with respect to a trained model, quantifying which inputs the model associates most strongly with anomalousness (Ribeiro et al., 2016; Lundberg & Lee, 2017). Root cause analysis (RCA) of anomalies instead seeks to identify the variables that actually cause the deviation in the underlying data-generating mechanism, by incorporating causal assumptions and reasoning (Budhathoki et al., 2022; Han et al., 2023; Orchard et al., 2025; Nguyen et al., 2024).

However, existing methods have thus far blurred the distinction between measurement and mechanistic outliers, despite its practical importance. To bridge this gap, we propose a causal formalization of measurement and mechanistic anomalies. Our framework allows us to not only identify which variables are responsible for deviations, but in addition, also determine whether an anomaly arises from a measurement error or a mechanism change.

Specifically, we interpret mechanistic and measurement anomalies as different interventions on the underlying

causal graph \mathcal{G} . The key difference from existing RCA methods is that we consider interventions on latent (“real”) and observed (“measured”) variables, respectively. Similar to existing RCA methods (Orchard et al., 2025), we leverage the Independence of Causal Mechanisms (ICM; Schölkopf et al., 2012; Peters et al., 2017), and in particular the *Sparse Mechanism Shift Hypothesis* (SMS; Schölkopf et al., 2021). It posits that explanations requiring multiple mechanisms to fail jointly are inherently unlikely. In our example in Fig. 1, this implies that interpreting \mathbf{m} as a measurement outlier (one failure) is more plausible than two concerted mechanism changes in $X \rightarrow Y$ and $Y \rightarrow Z$.

Since clean training data is often unavailable in practice, we consider the unsupervised in-sample setting, where anomalies must be identified directly within a given dataset. Our contributions are threefold: (i) We establish outlier types are identifiable up to observational equivalence in the infinite-sample limit. (ii) We introduce a maximum likelihood framework that enables efficient detection, localization, and attribution of anomalies. (iii) We develop a practical algorithm that achieves state-of-the-art performance on synthetic and real-world datasets in localization of root causes, and can additionally classify root causes as measurement and mechanistic anomalies.

2. Preliminaries

Throughout this paper, we assume a causal process over latent causal state variables $\mathbf{X}^* = (X_1^*, \dots, X_d^*)$, and observed features $\mathbf{X} = (X_1, \dots, X_d)$ which are readouts of these latent variables. We further assume that in a small fraction of the samples, the default generating process is violated in some way. We interchangeably refer to these samples as *outliers* or *anomalies*. We use bold capital letters such as \mathbf{X}^* , \mathbf{X} , \mathbf{W} , \mathbf{Z} to refer to sets of variables, and bold small letters such as \mathbf{x}^* , \mathbf{x} , \mathbf{z} , \mathbf{w} to refer to their i.i.d. samples.

2.1. Causal Model

Before describing the violations, we first describe the anomaly-free case. Let $\mathbf{V} = \mathbf{X}^* \cup \mathbf{X}$ be the full set of variables. We assume that the causal process is governed by a directed acyclic graph (DAG) $\mathcal{G} = (\mathbf{V}, E)$, where each edge $(V_j \rightarrow V_i) \in E$ encodes a direct causal influence. We write $\text{Pa}_j^* \subset \mathbf{X}^*$ for the latent parents of X_j^* , and denote by $\text{Pa}_j := \{X_k \in \mathbf{X} : X_k^* \in \text{Pa}_j^*\}$ the corresponding observed variables. By definition, every X_j only has one parent, the latent variable X_j^* . See Fig. 2a for an example.

When we speak of a *sink node*, we refer to a sink node among the induced subgraph $\mathcal{G}[\mathbf{X}^*]$, i.e. those features X_j^* that have no children in \mathbf{X}^* . Likewise, a *root node* is a feature X_j^* that has no parent among \mathbf{X}^* . To make our task feasible, we make the following standard assumptions on

the causal process (Pearl, 2009):

1. *Causal Sufficiency*: There are no hidden confounders affecting two or more variables of \mathbf{X}^* .
2. *Causal Faithfulness*: All independencies in the data are mirrored by d -separation in the graph.

Additionally, we assume that the data is generated by a structural causal model (SCM; Pearl, 2009), where each latent variable X_j^* is generated via a structural assignment with independent noise U_j and each observation X_j is a faithful measurement: $X_j^* = f_j(\text{Pa}_j^*, U_j)$, $X_j = X_j^*$.

Under these assumptions, the joint distribution factorizes in causal order:

$$P(\mathbf{X}^*, \mathbf{X}) = \prod_{j=1}^d P(X_j^* | \text{Pa}_j^*) P(X_j | X_j^*).$$

Under the clean process, the observed variables X_j accurately reflect the underlying causal structure of \mathcal{G} without distortion. An anomaly is then a sample in which this clean picture is violated.

2.2. Causal Anomalousness

Given an SCM, violations in the generating mechanisms of \mathbf{X}^* and \mathbf{X} can give rise to two different kinds of outliers. We assume that such violations can be represented by independent replacements of individual structural or measurement mechanisms, as follows:

Definition 2.1 (Mechanistic Anomalies). With probability $P(Z_j = 1) = \pi_j^{mech}$, the default structural assignment of X_j^* is replaced with an outlier distribution $P_{O_j^{mech}}$,

$$X_j^* = (1 - Z_j)f_j(\text{Pa}_j^*, U_j) + Z_j O_j^{mech},$$

with $Z_j \sim \text{Bernoulli}(\pi_j^{mech})$, $z_j \in \{0, 1\}$.

Definition 2.2 (Measurement Anomalies). With probability $P(W_j = 1) = \pi_j^{meas}$, the measurement mechanism of X_j is replaced with an outlier distribution $P_{O_j^{meas}}$,

$$X_j = (1 - W_j)X_j^* + W_j O_j^{meas},$$

with $W_j \sim \text{Bernoulli}(\pi_j^{meas})$, $w_j \in \{0, 1\}$.

Formally, the introduction of outlier distributions is equivalent to adding additional exogenous variables to the structural equations of \mathbf{X}^* and \mathbf{X} , analogous to the noise variables in a standard SCM. As is customary, we do not represent such exogenous variables in the causal DAG, and instead interpret the events $Z_j = 1$ and $W_j = 1$ as interventions on the anomaly-free X_j^* and X_j , respectively.

Interventions can be modeled as either *soft* or *hard* (Pearl, 2009). Soft interventions preserve (possibly altered) dependence on parent variables, whereas hard interventions

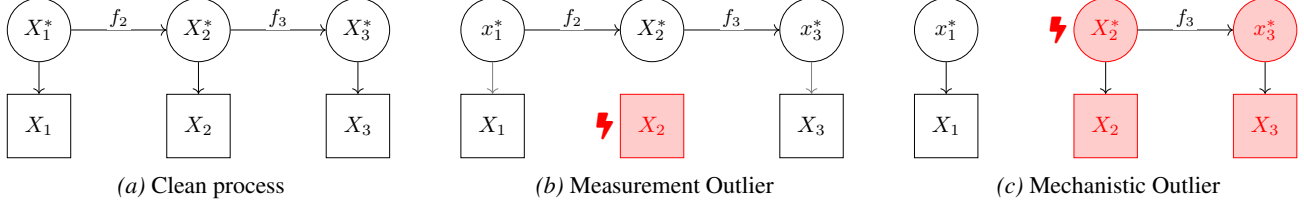


Figure 2. Different outlier types induce different downstream behavior. Red lightning symbols ⚡ indicate interventions that correspond to measurement outliers (on observed variables) and mechanistic outliers (on latent variables).

replace the structural assignment and remove all parent dependence. Because we assume anomalies to be rare—we might only observe a single sample of a specific failure type—parent-dependent deviations are statistically undetectable in finite samples. We therefore model anomalies as hard interventions, which captures deviations detectable at the sample level. To model parent-dependent mechanisms (e.g., $X_j^* := (1 - Z_j)f_j(\text{Pa}_j^*, U_j) + Z_j \cdot g_j(\text{Pa}_j^*, U_j)$) as in causal mixture models (Liu & Chan, 2015; Hu et al., 2018), we would require larger numbers of outliers.

Formally, we assume that $(\mathbf{O}^{mech}, \mathbf{O}^{meas}) \perp\!\!\!\perp (\mathbf{X}^*, \mathbf{X}) \mid (\mathbf{Z}, \mathbf{W}) = \mathbf{0}$, meaning that the outlier variables are independent of the anomaly-free data. Under this assumption, the structural replacements correspond to hard interventions on \mathcal{G} . Consequently, each sample $\mathbf{x}^{(i)}$ has its own corresponding true graph $\mathcal{G}^{(i)}$, which for non-anomalous samples is simply \mathcal{G} , and for anomalous samples is a mutilated graph in which the edges Pa_j^* into X_j^* (or X_j^* into X_j) have been removed (cf. Fig. 2b, 2c). We write $\mathcal{G}(\mathbf{a})$ to denote the graph induced by an outlier assignment $\mathbf{a} = (\mathbf{z}, \mathbf{w})$.

The crucial difference in the outlier types lies in how errors propagate. Since observed variables X_j never have children, a measurement error ($w_j = 1$) does not affect any descendants: the underlying X_j^* remains unchanged, and so do the downstream nodes. By contrast, mechanistic outliers in X_j^* replace f_j itself, affecting the marginal distributions of their downstream nodes. For instance, in Fig. 2b, X_2 is intervened upon but the causal relations $X_1^* \rightarrow X_2^* \rightarrow X_3^*$ remain intact. In contrast, in Fig. 2c, the mechanism that generates X_2^* changes, thereby perturbing the marginal distributions of all its downstream variables too.

Similar to prior work in root cause localization (Orchard et al., 2025), we adopt the assumption of Sparse Mechanism Shifts (SMS; Schölkopf et al., 2021), which posits that failures of individual mechanisms are rare and occur independently across features. Under the SMS assumption, explanations of the observed data that invoke fewer mechanism shifts are preferred. In our setting, the SMS assumption further implies that (\mathbf{W}, \mathbf{Z}) are jointly independent.

3. Theory

In this section, we formalize our theory for detecting, localizing, and classifying anomalies. We begin by showing *structural identifiability* in the infinite-sample limit: given the true DAG, anomalous samples can be recovered and classified (up to observational equivalence). This notion of identifiability deliberately focuses on the conditional independencies (CI) implied by the DAG, while ignoring distribution-dependent signals such as marginal shifts. The rationale is that CI constraints represent the minimal information available for outlier classification without imposing additional assumptions on the data-generating process, such as frequencies of outlier types or the functional form of their distributions. Next, because outliers are typically too rare for CI tests to detect, and the exponential search space creates a multiple testing problem, we propose a *latent maximum likelihood estimation (MLE)* framework to infer the latent outlier indicators from the observed data.

3.1. Structural Identifiability

We formalize the intuition that only outlier assignments that respect the CIs of the observed data are admissible. Since we model outliers with hard interventions, they induce distinctive dependency patterns, except in cases where different outlier configurations generate equivalent dependence structures among \mathbf{X} . For example, consider the latent dag $X_0^* \rightarrow X_1^* \rightarrow X_2^*$. A hard intervention on the latent variable X_1^* and a hard intervention on the observed X_0 induce identical CI constraints for the observed data. We define this notion of equivalence, as follows.

Definition 3.1 (Equivalence of DAGs). We call two DAGs \mathcal{G} and \mathcal{G}' **observationally equivalent**, $\mathcal{G} \equiv \mathcal{G}'$, if they imply the same CI constraints for the observed data \mathbf{X} .

Definition 3.2 (Structural equivalence of assignments). Let $\mathbf{A} = (\mathbf{Z}, \mathbf{W})$ and $\mathbf{A}' = (\mathbf{Z}', \mathbf{W}')$ be (latent) random assignments of outliers. We say that \mathbf{A} and \mathbf{A}' are **structurally equivalent** almost surely, $\mathbf{A} \equiv \mathbf{A}'$, if

$$P(\mathcal{G}(\mathbf{A}) \equiv \mathcal{G}(\mathbf{A}')) = 1.$$

Within an equivalence class of outlier combinations that induce the same dependencies, we can further use the

SMS assumption to break ties, which enables differentiation in additional cases, such as the example in the introduction. The simplest case of observational equivalence is sink nodes. Since they have no children, interventions on the latent variables induce the same CI constraints as interventions on the observed variables. For non-equivalent cases, the combination of DAG and observed data provide a clear signal. An assignment is only admissible if the observed data matches the implied constraints in every cluster, which we formalize in the next definition.

Definition 3.3 (Respect of CI constraints). A (latent) random assignment \mathbf{A} is said to **respect its CI constraints** if for almost every assignment value \mathbf{a} and every measurable subset $S \subseteq \{\mathbf{A} = \mathbf{a}\}$ with $P(S) > 0$, the conditional distribution of \mathbf{X} on S , $P_{\mathbf{X}|S}$, is faithful to the induced $\mathcal{G}(\mathbf{a})$.

Consider a bivariate graph $X_1 \rightarrow X_2$ and an assignment of $\mathbf{z} = (0, 1), \mathbf{w} = (0, 0)$ for a positive-measure subset of points. To be admissible, *every positive-measure subset* of this selection must satisfy the conditional independencies implied by the induced DAG $\mathcal{G}(\mathbf{a})$. This requirement rules out assignments that mix different types of points in a way that masks dependencies. For instance, if only half of the assigned points were generated under $\mathbf{z} = (0, 1), \mathbf{w} = (0, 0)$, whereas the other half of the assigned points were generated under $\mathbf{z} = (0, 0), \mathbf{w} = (0, 0)$, then in the combined set we would have $X_1 \not\perp\!\!\!\perp X_2$. Only by checking faithfulness in every positive-measure subset these cancellations can be avoided. With everything in place, we can now state the identifiability result.

Theorem 3.4 (Structural Identifiability). *Let \mathbf{A} be the true assignment, and let \mathbf{A}' be an arbitrary latent assignment. Suppose that, for almost every assignment value \mathbf{a} , the conditional distribution $P_{\mathbf{X}|\mathbf{A}=\mathbf{a}}$ is faithful to $\mathcal{G}(\mathbf{a})$. Then we have that \mathbf{A}' respects its CI constraints almost surely, if and only if \mathbf{A}' is structurally equivalent to \mathbf{A} almost surely.*

We provide the proof in Appx. A.1.1. The theorem characterizes identifiability in an idealized, infinite-sample regime, where all CI relations implied by the data-generating process are observable. In principle, one might consider using CI tests to reject inadmissible latent assignments. However, such an approach is fundamentally impractical. First, in finite samples, a latent assignment \mathbf{A} may include a small number of outlier points—possibly even a single observation—making the corresponding conditional dependencies statistically undetectable. Second, even ignoring the multiple-testing problem due to the exponential search space of assignments, the subset-level faithfulness in Def. 3.3 is inherently undetectable in finite samples.

For these reasons, we instead adopt a maximum likelihood estimation (MLE) approach, which allows efficient heuristic optimization over the space of assignments while im-

licitly respecting the structural constraints of the model.

3.2. Latent Maximum Likelihood Estimation

In finite samples, anomalies are often too rare to reliably estimate separate distributions for all failure types. We therefore analyze anomalies at the level of individual points. Specifically, we assume access solely to an estimate of the clean density, obtained from the non-anomalous data. For post-interventional densities, we model anomalous variables explicitly by assuming simple priors (e.g., uniform). This enables us to compare likelihoods under different anomaly assignments without needing to learn distributions or dependencies for the post-interventional distributions. In Sec. 4, we propose an algorithm to learn this clean density.

By assigning each sample to the outlier assignment that yields the best likelihood, we implicitly leverage the structural constraints of Theorem 3.4, while additionally enabling detection of anomalies beyond purely structural changes. For instance, a mechanistic outlier at a root node may preserve the dependency structure while still inducing a detectable distributional shift. By modeling the outlier indicators (\mathbf{Z}, \mathbf{W}) as independent Bernoulli variables, we further favor sparse root causes in accordance with the SMS assumption.

To evaluate the likelihood of arbitrary outlier assignments, we require prior distributions $\tilde{P}_{O_j^{meas}}$ and $\tilde{P}_{O_j^{meas}}$ for anomalous variables, along with estimates \hat{p} of the conditional anomaly-free densities. Measurement outliers pose a computational challenge, as they require marginalization over latent clean values. We first describe this marginalization, before we present the MLE objective.

Marginalization For the outlier indicators \mathbf{z}, \mathbf{w} of sample \mathbf{x} , we define $\mathcal{Z}_{\mathbf{x}} = \{j : z_j = 1\}$, $\mathcal{W}_{\mathbf{x}} = \{j : w_j = 1\}$. By integrating out the latent values corresponding to measurement outliers, we obtain the density over the remaining observed features. The full density is thus given by multiplying this density with the outlier densities:

$$p(\mathbf{x}) = \underbrace{\prod_{j \in \mathcal{W}_{\mathbf{x}}} \tilde{P}_{O_j^{meas}}(x_j)}_{\text{Meas. density}} \left[\int \underbrace{\prod_{j \notin \mathcal{Z}_{\mathbf{x}}} \hat{p}(x_j | \text{pa}_j)}_{\text{'Clean' density}} \right. \\ \left. \underbrace{\prod_{j \in \mathcal{Z}_{\mathbf{x}}} \tilde{P}_{O_j^{mech}}(x_j)}_{\text{Mech. density}} \underbrace{\prod_{j \in \mathcal{W}_{\mathbf{x}}} dx_j}_{\text{Unobs. latent values}} \right]. \quad (1)$$

In general, the integral in Eq. (1) cannot be evaluated in closed form, but it can be approximated via Monte Carlo sampling. We explain how to do so in Sec. 4. Also, we noted above how outliers in sink nodes are indistinguishable based on CI constraints alone, we can see directly from

the marginalization that this remains the case if we assume equal priors for these variables.

We obtain the joint likelihood of $\mathbf{x}, \mathbf{z}, \mathbf{w}$ by multiplying with the intervention probabilities. We define $\text{Bern}(u; \pi) := \pi^u(1 - \pi)^{1-u}$, and get

$$\mathcal{L}(\mathbf{x}, \mathbf{a}; \boldsymbol{\pi}) = p(\mathbf{x}) \prod_{j=1}^d \text{Bern}(z_j; \pi_j^{\text{mech}}) \text{Bern}(w_j; \pi_j^{\text{meas}}).$$

If we revisit the introductory example in Fig. 1, we see that even without knowing the exact priors and distributions, modeling \mathbf{m} as a measurement outlier in Y probably yields a higher likelihood than modeling it as two mechanistic outliers in Y and Z . By marginalizing over Y , we get a clean density over X, W, Z . In contrast, proposing two mechanistic outliers would incur the cost of low outlier probabilities twice.

MLE objective Now that we know how to compute the likelihood for arbitrary assignments, our goal is the optimization over both intervention probabilities $\boldsymbol{\pi} = (\boldsymbol{\pi}^{\text{mech}}, \boldsymbol{\pi}^{\text{meas}})$ and assignments $\mathbf{A} = \{\mathbf{a}^{(i)}\}_{i=1}^N$

$$\arg \max_{\boldsymbol{\pi}, \mathbf{A}} \sum_{i=1}^N \log \mathcal{L}(\mathbf{x}^{(i)}, \mathbf{a}^{(i)}; \boldsymbol{\pi}). \quad (2)$$

This latent MLE is a mixture estimation problem: We have mixture components with unknown probabilities $\boldsymbol{\pi}$, and their distributions are induced by the clean SCM, the outlier assignments, and the prior outlier densities. Enumerating all assignments is exponential in d , but since outliers are rare and independent, we can use heuristic local search over features with low conditional likelihoods to obtain good local optima. We illustrate our instantiation in Sec. 4.

The approximate MLE yields a discrete outlier assignment \mathbf{A} , but often we want a continuous score that measures how strongly a feature is suspected to be a root cause. Since exact posteriors are intractable, we suggest a surrogate. We write $\mathbf{h}^{(j,k)}$ for \mathbf{h} with its j -th entry replaced by k , and write $\mathcal{L}_{z_j \rightarrow 1} := \mathcal{L}(\mathbf{x}, \mathbf{z}^{(j,1)}, \mathbf{w}^{(j,0)}; \boldsymbol{\pi})$, and $\mathcal{L}_{w_j \rightarrow 1} := \mathcal{L}(\mathbf{x}, \mathbf{z}^{(j,0)}, \mathbf{w}^{(j,1)}; \boldsymbol{\pi})$ for the likelihoods under the respective added outlier types. Based on these, we define our root cause score as:

$$\begin{aligned} \Delta_j &:= -\log \mathcal{L}(\mathbf{x}, \mathbf{z}^{(j,0)}, \mathbf{w}^{(j,0)}; \boldsymbol{\pi}) \\ &\quad + \log (\max(\mathcal{L}_{z_j \rightarrow 1}, \mathcal{L}_{w_j \rightarrow 1})) \end{aligned} \quad (3)$$

Here, Δ_j measures the gain in fit if x_j is treated as a root cause. Comparing the measurement and mechanistic assignment defines the *confidence*,

$$\tilde{C}_j := |\log \mathcal{L}_{z_j \rightarrow 1} - \log \mathcal{L}_{w_j \rightarrow 1}|. \quad (4)$$

The confidence approximates how much more likely a feature of our sample is one kind of outlier than the other, conditional on being a root cause.

4. Instantiation

Algorithm 1 CALI

Input: DAG \mathcal{G} , dataset \mathbf{X}
Output: anomaly assignment $\mathbf{A} = (\mathbf{Z}, \mathbf{W})$, feature scores \mathcal{S} , confidences \mathcal{C}

for all $X_k \in \mathcal{G}$ **do**
 $\hat{f}_k \leftarrow \text{ROBUSTLYREGRESS}(\text{Pa}_k, X_k)$
 $R_k \leftarrow X_k - \hat{f}_k(\text{Pa}_k)$
 $\mathcal{L}(R_k) \leftarrow \text{ESTIMATENOISE}(R_k)$

end for
 $\mathbf{A} \leftarrow \text{MLE-ASSIGN}(\mathbf{X}, \mathcal{G}, \{\hat{f}_k\}, \{\mathcal{L}(R_k)\})$
 $\mathcal{S} \leftarrow \text{SCORE}(\mathbf{A}, \mathbf{X}, \mathcal{G}, \{\hat{f}_k\}, \{\mathcal{L}(R_k)\})$ (Eq. (3))
 $\mathcal{C} \leftarrow \text{CONF}(\mathbf{A}, \mathbf{X}, \mathcal{G}, \{\hat{f}_k\}, \{\mathcal{L}(R_k)\})$ (Eq. (4))

return $\mathbf{A}, \mathcal{S}, \mathcal{C}$

With the theoretical background established in the previous section, we introduce our method CALI,¹ a heuristic algorithm for the maximization in Eq. (2). We assume that we are provided an estimate $\hat{\mathcal{G}}$ of the true DAG, which could either be estimated from observed data or provided by a domain expert. In principle, the anomaly-free density could be approximated using different causal models; here, we adopt an additive noise model (ANM) for tractable estimation of conditional densities under contamination. Given $\hat{\mathcal{G}}$, we approximate the SCM with robust regression functions and contamination-aware estimation of noise distributions. We illustrate the algorithm in Alg. 1. Here, we present the main building blocks at a high level; we provide further details, pseudocode, and complexity analysis in Appx. A.2.

ROBUSTLYREGRESS estimates a function $\hat{f}_j : \mathbb{R}^k \rightarrow \mathbb{R}$ for each node X_j with k parent nodes Pa_j . We use Generalized Additive Models (GAMs; [Hastie, 2017](#)) with cubic spline bases to model the mechanisms. To improve robustness to outliers, we adopt the quantile regression approach of [Fasiolo et al. \(2021\)](#), fitting the mechanisms via median regression. For each node X_j , we then define the residuals of the fitted causal mechanism as $r_j = x_j - \hat{f}_j(\text{pa}_j)$. To model the distribution of these residuals robustly in the presence of outliers, we use a trimmed kernel density estimation approach, in which a fraction α of the observations farthest from the median are discarded prior to fitting a Gaussian kernel density estimator ([Parzen, 1962](#)).

MLE-ASSIGN optimizes Eq. (2) heuristically. For likelihood evaluations under a given assignment, we use a Monte Carlo (MC) approximation of the integral over the unob-

¹Causal Anomaly Localization and Inspection

served "clean" values in Eq. 1, and prior distributions for the post-interventional variables. For the outlier distributions, we use uniform densities over the observed feature ranges. For the MC approximation, we can sample random latent values for each $j \in \mathcal{W}$ from $\hat{P}(X_j | \text{Pa}_j = \text{pa}_j)$. For each such sample, we evaluate the densities of the remaining terms in the integral, and approximate the marginalized likelihood by averaging across samples (see Appx. A.2.2).

Given these ingredients, MLE-ASSIGN starts from an empty assignment with all Bernoulli probabilities set to zero, i.e., all clean samples. We prioritize candidate root causes based on how low their residual likelihoods under the clean density are. Candidates are only added to the assignment if it increases the sample likelihood enough to justify an increase of the respective Bernoulli probability globally. This heuristic is greedy: we iteratively accept assignments until no further improvement is possible, reducing the search complexity from exponential to linear in the number of features. Despite its simplicity, we demonstrate in Sec. 6 that this approach performs well in practice because rare, independent outliers interact minimally, making independent optimization near-optimal.

5. Related Work

In this section, we situate our work within the literature on causal reasoning for outlier analysis; an overview of unsupervised outlier detection and non-causal feature attribution is provided in Appx. A.5.

Root Cause Analysis (RCA) aims to identify the causal factors that most directly explain a target outcome of interest, ranging from treatment effects to system failures (Li et al., 2022; Strobl & Lasko, 2023a;b; Strobl, 2024; Pham et al., 2024; Li et al., 2025; Ikram et al., 2025).

Recent work has instantiated RCA for anomaly detection. Budhathoki et al. (2022) assume a known structural causal model (SCM) and attribute feature-level contributions using Shapley values, which was adopted in subsequent RCA work (Strobl & Lasko, 2023a;b). Han et al. (2023) propose a causal VAE for anomaly localization. Orchard et al. (2025) assume a polytree-structured DAG and identify root causes via marginal outlier scores. However, these approaches primarily identify *where* anomalies originate, without explaining *how* they occur. We address this gap by extending the causal framework to jointly model and differentiate the two principal categories of measurement and mechanistic outliers.

Separately, in the time series literature, heuristic distinctions between "sensor" and "process" anomalies have been proposed (Salem et al., 2013; Haque et al., 2015; Bachechi et al., 2022; LaRosa et al., 2022). These methods rely on correlation-based criteria or domain knowledge rather than

an explicit causal formalization. The closest such approach distinguishes "cyber" and "measurement" anomalies using Granger causality (Sun et al., 2025), which captures predictive temporal dependencies rather than interventional causal structure. The method is further restricted to time series data and assumes sufficient samples per failure mode. In contrast, our algorithm detects, localizes, and classifies heterogeneous failure types even with as little as a single sample per type on i.i.d. data.

6. Experiments

In this section, we empirically evaluate CALI across various settings. In particular, we answer three main questions:

1. How well does CALI *localize* root causes?
2. How well does CALI *classify* outlier types?
3. How does CALI perform in a Case Study on real-world data with interpretable features?

In addition, we conduct several supplementary experiments, including an evaluation of the detection capabilities of CALI, its sensitivity to sample size and feature dimensionality, and its runtime (see Appx. A.6).

Data To be able to evaluate on data with known ground truth, we generate 2000 samples \mathbf{x} from an SCM defined over a random Erdős–Rényi DAG with 15 nodes. Each variable X_j is specified as $X_j = f_j(\text{Pa}(X_j)) + U_j$, where f_j is a quadratic or cubic polynomial and $U_j \sim \mathcal{N}(0, \sigma^2)$. For 10% of samples, outliers are injected by shifting the marginal distribution of X_j by k empirical standard deviations and replacing the actual value with a random sample from the shifted marginal distribution. In our plots we refer to k as outlier strength. For mechanistic outliers, the values of downstream nodes are recomputed with new noise.

In addition, we evaluate on two real-world datasets with known consensus DAGs: the Sachs dataset (Sachs et al., 2005) and the *Causal Chambers* benchmark (Gamella et al., 2025). Both contain observational and interventional data. In Causal Chambers, interventions are applied at different strengths (*mid* and *strong*), whereas interventions in the Sachs dataset induce weaker marginal shifts than the *mid* interventions. We simulate mechanistic outliers by injecting a small fraction of interventional samples, and measurement outliers by replacing individual features with values drawn from the post-intervention distribution. We consider three settings with respect to outlier strength: low (Sachs), medium (Causal Chambers, *mid*), and high (Causal Chambers, *strong*). Further details on data-generation and processing are provided in Appx. A.4.

Instantiation of CALI CALI requires a causal graph G to be specified. We consider two variants. First, to eval-

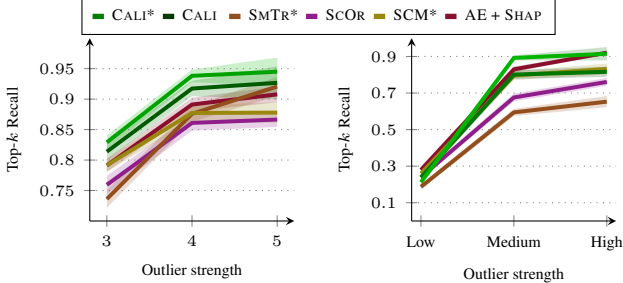


Figure 3. Root Cause Localization (Top- k recall, higher is better) for synthetic data (left) and real data (right). Outlier strength corresponds to mean shifts in terms of standard deviations (left), or the relative strength of intervention (right): low (Sachs), medium (Causal Chamber, *mid*), high (Causal Chamber, *strong*). We set k to the true number of root causes in each sample. Shaded regions indicate 95% confidence intervals across 20 runs.

ate the best possible performance, we consider CALI with access to the true causal graph \mathcal{G}^* . Second, as \mathcal{G}^* is often unknown, we consider the realistic case where CALI is given a learned causal DAG. To this end, we apply CALI to the outputs of various causal discovery algorithms on independently generated synthetic datasets and assess downstream performance (see Appx. A.6.7). The best performance occurs with NoGAM (Montagna et al., 2023), with AE-based prefiltering, which we thus use for subsequent experiments. We write CALI* for when it has access to the true graph, and CALI when the causal graph is learned.

Evaluation Metrics For root cause localization, we report Top- k Recall, where k is set dynamically to the true number of root causes of the respective sample, which calculates what percentage of the true root causes is included in the top k candidates. This metric is detection-agnostic and ensures a fair comparison across methods. However, it does not necessarily reflect performance in deployment, as explaining anomalies that are not detected provides no actionable insight. Therefore, we also report an evaluation that takes detectability into account in Appx. A.6.1, which also includes further metrics.

For the classification of outlier types, we report the accuracy over correctly detected root causes, evaluating the classification performance for actionable anomalies.

6.1. Root cause localization

To investigate how well CALI performs compared to existing root cause analysis methods. We grant all methods access to the ground truth DAG where applicable and mark such methods with a *. We consider SCM* an adapted version of SCM-based attribution approaches (Budhathoki et al., 2022; Strobl & Lasko, 2023a;b), SMTR* and

SCOR² (Orchard et al., 2025), and AE-SHAP (autoencoder with Shapley values). We refer to Appx. A.3 for detailed implementations and hyperparameter selection. Since all competitors assume a given split between the normal and anomalous regimes, and are thus not directly applicable in the in-sample setting, we combine them with the best-performing sample detector aside from CALI to obtain the split (see Appx. A.3).

We evaluate all methods and report the results in Fig. 3. On synthetic data, CALI* achieves the highest performance, with CALI using a learned graph as a close second. On the real-world datasets, all methods struggle under the weak outliers in the Sachs dataset, resulting in uniformly low Top- k recall. In contrast, on the Causal Chambers dataset, CALI* already attains a Top- k recall of 90% under the medium outlier strength, a level that is only matched by a single competitor under strong outliers.

Notably, this evaluation measures root-cause localization under oracle detection. When we take detectability into account (see Appx. A.6.4), CALI* and CALI outperform competing approaches by an even larger margin.

6.2. Outlier type classification

Next, we evaluate whether CALI can accurately classify the types of detected root causes. As a baseline, we consider MARG, which identifies outlier types using marginal outlieriness. A root cause is classified as a measurement outlier if none of its child values exceed a predefined outlieriness threshold. A key limitation of this baseline is the difficulty of threshold selection. Since we want to eliminate errors in causal discovery for the comparison, we only consider CALI* and MARG* for this experiment. We provide the results with learned graphs is provided in Appx. A.6.6.

To ensure a fair comparison, we provide MARG* with the root causes identified by CALI* and tune its significance threshold on synthetic data. Detailed implementation and hyperparameter selection are described in Appx. A.3. Fig. 4 shows that CALI* outperforms MARG*. Despite the poor localization performance on the Sachs dataset, those root causes that are correctly identified are classified with high accuracy. Especially under weak outliers CALI beats MARG by a large margin. Another major advantage of CALI is that it performs robustly across different settings without requiring a threshold, as we further illustrate in the “influence of degree” experiment in Appx. A.6.6.

6.3. Case Study on NYC Taxi Data

To qualitatively verify the anomalies that CALI finds in real data, we perform a case study on the NYC Yellow Taxi Trip

²Short for SMOOTHTRAVERSAL, SCOREORDER

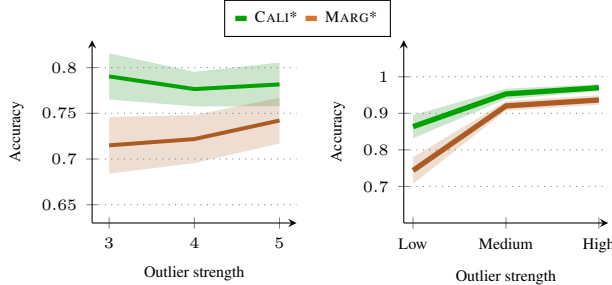


Figure 4. Classification accuracy (higher is better) of outlier types for synthetic data (left) and real world data (right). Outlier strength corresponds to mean shifts in terms of standard deviations (left), or the relative strength of intervention (right): low (Sachs), medium (Causal Chamber, *mid*), high (Causal Chamber, *strong*). Random guessing corresponds to 50%. Shaded regions indicate 95% confidence intervals across 20 runs.

Dataset (Elemento, n.d.), which contains 12.7 million taxi trips with pickup and dropoff coordinates, times, fares, tips, extra charges, and the applied rate. We run CALI on a random subset of 5 000 entries using a selected set of continuous features. We illustrate the DAG used in the analysis in Fig. 5, and the examples identified by CALI in Tab. 1 and Tab. 2. By filtering the root causes by types, and sorting based on gain and confidence we selected 3 anomalies with high likelihood gain and high classification confidence. For simplicity, we convert the coordinates into air distance.

First, we look into the measurement outliers (Tab. 1). The first and third examples have recorded travel times of 94 and 33 minutes and distances of 3.9 and 0.6 miles, respectively, but especially the fares (10 and 5) are suspiciously low compared to what one would expect from accrued time-based charges alone. This inconsistency between distance, time, and fare, makes an incorrectly recorded travel time by far the most plausible explanation. The second example in Tab. 1 is perhaps even more clearly a measurement error: the trip distance of 9.4 miles is incompatible with the air distance that follows from the pickup and drop-off coordinates, time, and fare, all of which instead indicate a very short trip.

Next, we consider the mechanistic outliers in Tab. 2. The first example has a fare that is unusually high for a trip of less than a minute and zero-distance, yet consistent with the total amount and tip, reflecting a possibly fraudulent trans-

Table 1. Top 3 measurement outliers CALI identifies on the NYC Taxi Dataset, ranked by confidence, among the 30 highest gains. Detected root cause is marked in bold.

Distance	Air Dist	Time	Fare	Tip	Total
3.90	3.1622	94.65	10.00	2.00	13.30
9.40	0.0021	0.20	2.50	0.00	3.30
0.60	0.9782	33.52	5.00	0.00	6.30

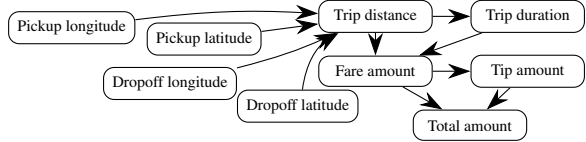


Figure 5. Causal relationships of the NYC Taxi Dataset.

action. The second and third samples are textbook definitions of a mechanistic outlier as metadata indicates that these are rides not under the regular mechanism, but under the JFK flat fare, which sets a fixed fare of \$52 independent of distance or time.

Overall, we find that CALI successfully identifies measurement and mechanistic outliers in real-world data, with explanations that are plausible and actionable.

7. Conclusion

We studied explainable anomaly detection through a causal lens, distinguishing measurement errors from genuine mechanistic anomalies by modeling both as hard interventions. We cast the problem as latent MLE and introduced a practical algorithm that performs root cause localization on par with prior methods, while additionally enabling outlier type classification. Finally, we demonstrated in a case study that our approach produces interpretable and plausible anomaly characterizations.

Limitations CALI requires a given DAG, and performance depend on how well the true mechanisms, noise model, and outlier types fit our modelling assumptions. If the DAG is unknown, we have to estimate it using a causal discovery method. By doing so, we inherit the limitations of that method, potentially exacerbated by contamination. CALI is restricted to tabular data, although its main ideas can be extended to other data types.

Future Work Relaxing the strict causal setting can broaden applicability at a cost of precision. Another promising direction is causal discovery under contamination. Measurement outliers distort causal signals, mechanistic outliers carry useful information, and distinguishing these will likely benefit structure learning.

Table 2. Top 3 mechanistic outliers CALI identifies on the NYC Taxi Dataset, ranked by confidence, among the 30 highest gains. Detected root cause is marked in bold.

Distance	Air Dist	Time	Fare	Tip	Total
0.00	0.0559	0.75	220.00	44.05	264.35
0.00	0.0004	0.30	52.00	0.00	58.13
1.80	1.3863	8.48	52.00	11.63	69.76

References

Angiulli, F., Fassetti, F., Nisticò, S., and Palopoli, L. Explaining outliers and anomalous groups via subspace density contrastive loss. *Machine Learning*, 113:7565–7589, 2024.

Bachechi, C., Rollo, F., and Po, L. Detection and classification of sensor anomalies for simulating urban traffic scenarios. *Cluster Computing*, 25(4):2793–2817, 2022.

Breunig, M. M., Kriegel, H.-P., Ng, R. T., and Sander, J. LOF: identifying density-based local outliers. In *Proceedings of the ACM International Conference on Management of Data (SIGMOD)*, pp. 93–104. ACM, 2000.

Budhathoki, K., Minorics, L., Blöbaum, P., and Janzing, D. Causal structure-based root cause analysis of outliers. In *International conference on machine learning*, pp. 2357–2369. PMLR, 2022.

Bühlmann, P., Peters, J., and Ernest, J. Cam: Causal additive models, high-dimensional order search and penalized regression. *The Annals of Statistics*, 42, 2014.

Chandola, V., Banerjee, A., and Kumar, V. Anomaly detection: A survey. *ACM computing surveys (CSUR)*, 41(3): 1–58, 2009.

Crenshaw, J. F., Kalmbach, J. B., Gagliano, A., Yan, Z., Connolly, A. J., Malz, A. I., Schmidt, S. J., Collaboration, L. D. E. S., et al. Probabilistic forward modeling of galaxy catalogs with normalizing flows. *The Astronomical Journal*, 168(2):80, 2024.

Elemento. NYC Yellow Taxi Trip Data. <https://www.kaggle.com/datasets/elemento/nyc-yellow-taxi-trip-data>, n.d. Kaggle dataset (accessed 2025-11-11).

Fasiolo, M., Wood, S. N., Zaffran, M., Nedellec, R., and Goude, Y. qgam: Bayesian nonparametric quantile regression modeling in r. *Journal of Statistical Software*, 100:1–31, 2021.

Friedman Antwarg, L., Miller, R., Shapira, B., and Rokach, L. Explaining anomalies detected by autoencoders using Shapley Additive Explanations. *Expert Systems with Applications*, 186:115736, 2021.

Gamella, J. L., Peters, J., and Bühlmann, P. Causal chambers as a real-world physical testbed for AI methodology. *Nature Machine Intelligence*, 7(1):107–118, 2025.

Han, X., Zhang, L., Wu, Y., and Yuan, S. On Root Cause Localization and Anomaly Mitigation through Causal Inference. In *Proceedings of the 32nd ACM International Conference on Information and Knowledge Management, CIKM '23*, pp. 699–708, New York, NY, USA, 2023. Association for Computing Machinery.

Haque, S. A., Rahman, M., and Aziz, S. M. Sensor anomaly detection in wireless sensor networks for healthcare. *Sensors*, 15(4):8764–8786, 2015.

Hastie, T. J. Generalized additive models. *Statistical models in S*, pp. 249–307, 2017.

Hu, S., Chen, Z., Partovi Nia, V., Chan, L., and Geng, Y. Causal inference and mechanism clustering of a mixture of additive noise models. *Advances in neural information processing systems*, 31, 2018.

Ikram, A., Lee, K., Agarwal, S., Saini, S. K., Bagchi, S., and Kocaoglu, M. Root cause analysis of failures from partial causal structures. In *The 41st Conference on Uncertainty in Artificial Intelligence*, 2025.

Kingma, D. P. and Welling, M. Auto-Encoding Variational Bayes. *ArXiv*, abs/1312.6114, 2013.

LaRosa, N., Farber, J., Venkatasubramaniam, P., Blum, R., and Al Rashdan, A. Separating sensor anomalies from process anomalies in data-driven anomaly detection. *IEEE Signal Processing Letters*, 29:1704–1708, 2022.

Li, J., Chu, B. B., Scheller, I. F., Gagneur, J., and Maathuis, M. H. Root cause discovery via permutations and cholesky decomposition. *Journal of the Royal Statistical Society Series B: Statistical Methodology*, 2025.

Li, M., Li, Z., Yin, K., Nie, X., Zhang, W., Sui, K., and Pei, D. Causal inference-based root cause analysis for online service systems with intervention recognition. In *Proceedings of the 28th ACM SIGKDD Conference on Knowledge Discovery and Data Mining*, pp. 3230–3240, 2022.

Li, Z., Zhao, Y., Botta, N., Ionescu, C., and Hu, X. CO-POD: Copula-Based Outlier Detection . In *2020 IEEE international conference on data mining (ICDM)*, pp. 1118–1123. IEEE, 2020.

Li, Z., Zhu, Y., and Van Leeuwen, M. A Survey on Explainable Anomaly Detection. *ACM Transactions on Knowledge Discovery from Data*, 18(1):1–54, 2023.

Liu, F. and Chan, L. Causal discovery on discrete data with extensions to mixture model. *ACM Transactions on Intelligent Systems and Technology (TIST)*, 7(2):1–19, 2015.

Liu, F. T., Ting, K. M., and Zhou, Z.-H. Isolation forest. In *Proceedings of the IEEE International Conference on Data Mining (ICDM)*, pp. 413–422. IEEE, 2008.

Lundberg, S. M. and Lee, S.-I. A unified approach to interpreting model predictions. *Advances in neural information processing systems*, 30, 2017.

Mahalanobis, P. C. On the generalized distance in statistics. *Proceedings of the National Institute of Sciences of India*, 2(1):49–55, 1936.

Montagna, F., Noceti, N., Rosasco, L., Zhang, K., and Locatello, F. Causal discovery with score matching on additive models with arbitrary noise. In *Conference on Causal Learning and Reasoning*, pp. 726–751. PMLR, 2023.

Mothilal, R. K., Sharma, A., and Tan, C. Explaining Machine Learning Classifiers through Diverse Counterfactual Explanations. In *Proceedings of the 2020 Conference on Fairness, Accountability, and Transparency*, FAT* ’20, pp. 607–617, New York, NY, USA, 2020. Association for Computing Machinery.

Nguyen, P., Tran, T., Gupta, S., Nguyen, T., and Venkatesh, S. Root Cause Explanation of Outliers under Noisy Mechanisms. *Proceedings of the AAAI Conference on Artificial Intelligence*, 38:20508–20515, 2024.

Orchard, W. R., Okati, N., Mejia, S. H. G., Blöbaum, P., and Janzing, D. Root Cause Analysis of Outliers with Missing Structural Knowledge. In *The Thirty-ninth Annual Conference on Neural Information Processing Systems*, 2025.

Pang, G., Shen, C., Cao, L., and Hengel, A. Deep Learning for Anomaly Detection: A Review. *ACM Computing Surveys*, 54:1–38, 2021.

Parzen, E. On estimation of a probability density function and mode. *The annals of mathematical statistics*, 33(3): 1065–1076, 1962.

Pearl, J. *Causality: Models, Reasoning and Inference*. Cambridge University Press, 2nd edition, 2009.

Peters, J., Janzing, D., and Schölkopf, B. *Elements of causal inference: foundations and learning algorithms*. The MIT press, 2017.

Pham, L., Ha, H., and Zhang, H. Baro: Robust root cause analysis for microservices via multivariate bayesian online change point detection. *Proceedings of the ACM on Software Engineering*, 1(FSE):2214–2237, 2024.

Rezende, D. J. and Mohamed, S. Variational inference with normalizing flows. *ArXiv*, abs/1505.05770, 2015.

Ribeiro, M. T., Singh, S., and Guestrin, C. Why Should I Trust You?: Explaining the Predictions of Any Classifier. In *Proceedings of the 22nd ACM SIGKDD International Conference on Knowledge Discovery and Data Mining*, KDD ’16, pp. 1135–1144, New York, NY, USA, 2016. Association for Computing Machinery.

Rolland, P., Cevher, V., Kleindessner, M., Russell, C., Janzing, D., Schölkopf, B., and Locatello, F. Score matching enables causal discovery of nonlinear additive noise models. In *International Conference on Machine Learning*, pp. 18741–18753. PMLR, 2022.

Ruff, L., Vandermeulen, R., Goernitz, N., Deecke, L., Sidiqui, S. A., Binder, A., Müller, E., and Kloft, M. Deep One-Class Classification. In *International conference on machine learning*, pp. 4393–4402. PMLR, 2018.

Sachs, K., Perez, O., Pe’er, D., Lauffenburger, D. A., and Nolan, G. P. Causal protein-signaling networks derived from multiparameter single-cell data. *Science*, 308 (5721):523–529, 2005.

Sakurada, M. and Yairi, T. Anomaly Detection Using Autoencoders with Nonlinear Dimensionality Reduction. In *Proceedings of the 2nd Workshop on Machine Learning for Sensory Data Analysis (MLSDA)*, pp. 4–11. ACM, 2014.

Salem, O., Guerassimov, A., Mehaoua, A., Marcus, A., and Furht, B. Sensor fault and patient anomaly detection and classification in medical wireless sensor networks. In *2013 IEEE international conference on communications (ICC)*, pp. 4373–4378. IEEE, 2013.

Schölkopf, B., Platt, J., Shawe-Taylor, J., Smola, A., and Williamson, R. Estimating the Support of a High-Dimensional Distribution. *Neural Computation*, 13: 1443–1471, 2001.

Schölkopf, B., Janzing, D., Peters, J., Sgouritsa, E., Zhang, K., and Mooij, J. On causal and anticausal learning. *arXiv preprint arXiv:1206.6471*, 2012.

Schölkopf, B., Locatello, F., Bauer, S., Ke, N. R., Kalchbrenner, N., Goyal, A., and Bengio, Y. Towards Causal Representation Learning. *ArXiv*, abs/2102.11107, 2021.

Silverman, B. W. *Density estimation for statistics and data analysis*. Routledge, 2018.

Strobl, E. and Lasko, T. A. Sample-specific root causal inference with latent variables. In *Conference on Causal Learning and Reasoning*, pp. 895–915. PMLR, 2023a.

Strobl, E. V. Counterfactual formulation of patient-specific root causes of disease. *Journal of Biomedical Informatics*, 150:104585, 2024.

Strobl, E. V. and Lasko, T. A. Identifying patient-specific root causes with the heteroscedastic noise model. *Journal of Computational Science*, 72:102099, 2023b.

Sun, Y., Blum, R. S., and Venkatasubramaniam, P. Unifying Explainable Anomaly Detection and Root

Cause Analysis in Dynamical Systems. *arXiv preprint arXiv:2502.12086*, 2025.

Wachter, S., Mittelstadt, B. D., and Russell, C. Counterfactual Explanations Without Opening the Black Box: Automated Decisions and the GDPR. *Cybersecurity*, 2017.

Xu, S., Mameche, S., and Vreeken, J. Information-theoretic causal discovery in topological order. In *The 28th International Conference on Artificial Intelligence and Statistics*, 2025.

Zhao, Y., Nasrullah, Z., and Li, Z. Pyod: A python toolbox for scalable outlier detection. *Journal of machine learning research*, 20:1–7, 2019.

Zheng, X., Dan, C., Aragam, B., Ravikumar, P., and Xing, E. Learning sparse nonparametric dags. In *International conference on artificial intelligence and statistics*, pp. 3414–3425. Pmlr, 2020.

A. Appendix

A.1. Theory

In this appendix, we provide the proof of Theorem 3.4, and an example for observational equivalence classes.

A.1.1. PROOFS

We prove the statement of Theorem 3.4:

Theorem (Structural Identifiability). *Let \mathbf{A} be the true assignment, and let \mathbf{A}' be an arbitrary latent assignment. Suppose that, for almost every assignment value \mathbf{a} , the conditional distribution $P_{\mathbf{X}|\mathbf{A}=\mathbf{a}}$ is faithful to $\mathcal{G}(\mathbf{a})$. Then we have that \mathbf{A}' respects its CI constraints almost surely, if and only if \mathbf{A}' is structurally equivalent to \mathbf{A} almost surely.*

Proof of Theorem 3.4. Let \mathbf{A} be the true assignment, and let \mathbf{A}' be an arbitrary latent assignment. Suppose that, for almost every assignment value \mathbf{a} , the conditional distribution $P_{\mathbf{X}|\mathbf{A}=\mathbf{a}}$ is faithful to $\mathcal{G}(\mathbf{a})$.

We first show that if \mathbf{A}' respects its CI constraints almost surely, then \mathbf{A}' is structurally equivalent to \mathbf{A} almost surely. Suppose that \mathbf{A}' were not structurally equivalent to \mathbf{A} . Then, by Definition 3.2, there exists a measurable set S with $P(S) > 0$ such that the induced interventional DAGs are not observationally equivalent on S . Since the set of combinations of generating and assigned assignments $(\mathbf{a}, \mathbf{a}')$ is countable, at least one combination has to have positive measure on S . Thus, we can without loss of generality pick S such that a single configuration \mathbf{a} of the true assignment \mathbf{A} generated the data and a single configuration \mathbf{a}' of \mathbf{A}' is assigned.

By faithfulness, the distribution of \mathbf{X} restricted to S satisfies exactly the CI constraints implied by $\mathcal{G}(\mathbf{a})$. Since $\mathcal{G}(\mathbf{a})$ and $\mathcal{G}(\mathbf{a}')$ are not observationally equivalent, there exists at least one CI constraint implied by $\mathcal{G}(\mathbf{a}')$, that the distribution $P_{\mathbf{X}|S}$ violates.

This contradicts the assumption that \mathbf{A}' respects its CI constraints, which requires $P_{\mathbf{X}|S}$ to be faithful to $\mathcal{G}(\mathbf{a}')$ for any positive-measure set S for which $\mathbf{A}' = \mathbf{a}'$. Therefore, \mathbf{A}' must be structurally equivalent to \mathbf{A} almost surely.

Now we show that if \mathbf{A}' is structurally equivalent to \mathbf{A} almost surely, then \mathbf{A}' respects its CI constraints almost surely. Since \mathbf{A}' is structurally equivalent to \mathbf{A} almost surely, it follows that for almost every configuration \mathbf{a} , the induced DAGs $\mathcal{G}(\mathbf{a})$ and $\mathcal{G}(\mathbf{a}')$ are observationally equivalent. Thus, for any positive-measure subset S with $\mathbf{A}' = \mathbf{a}'$, we have that $P_{\mathbf{X}|S}$ is faithful to $\mathcal{G}(\mathbf{a})$ by assumption, which further implies that the distribution is also faithful to $\mathcal{G}(\mathbf{a}')$. This satisfies the definition of \mathbf{A}' respecting its CI constraints, and thus completes the proof. \square

A.1.2. EXAMPLES

As an example of observational equivalence classes, we consider the simple bivariate chain $X_1^* \rightarrow X_2^*$ with observed measurements X_1, X_2

Example 1 (Observational equivalence in the bivariate setting). Consider the simple DAG with two latent variables $X_1^* \rightarrow X_2^*$ and observed measurements X_1, X_2 . For clarity, write an assignment as $(Z_1, Z_2, W_1, W_2) = (z_1, z_2, w_1, w_2)$.

We only discuss the *dependency* between the observed variables X_1 and X_2 , since this is the level on which Theorem 3.4 operates. There are five cases (plus combinations thereof), which we analyze one by one:

- **No outliers:** $(0, 0, 0, 0)$. The chain is intact, so the observed pair is dependent

$$X_1 \not\perp\!\!\!\perp X_2.$$

- **Mechanistic outlier at X_1^* :** $(1, 0, 0, 0)$. A (hard) mechanistic intervention replaces X_1^* by an independent draw but leaves the structural equation for X_2^* intact, so X_2^* (and hence X_2) still depends on the intervened X_1^* . Therefore, the observed pair remains dependent

$$X_1 \not\perp\!\!\!\perp X_2.$$

(Remark: the marginal distribution of X_1 may change, but we only rely on the change/no-change of the dependency here. Since samples are drawn i.i.d, this can only materialize when dependencies *between variables* change.)

- **Measurement outlier at X_1 :** $(0, 0, 1, 0)$. Here the edge $X_1^* \rightarrow X_1$ is severed: the observed X_1 is generated independently of the latent X_1^* that drives X_2^* . Consequently the observed pair becomes independent

$$X_1 \perp\!\!\!\perp X_2.$$

- **Mechanistic outlier at X_2^* :** $(0, 1, 0, 0)$. A hard mechanistic intervention on X_2^* severs its dependence on the parent X_1^* . Hence X_2 is independent of X_1

$$X_1 \perp\!\!\!\perp X_2.$$

- **Measurement outlier at X_2 :** $(0, 0, 0, 1)$. Severing the measurement edge $X_2^* \rightarrow X_2$ makes the observed X_2 independent of X_1^* (and thus of X_1)

$$X_1 \perp\!\!\!\perp X_2.$$

Conclusion (observable CI patterns). From the perspective of observable dependence between X_1 and X_2 , the assignments fall into two classes.

Dependent class: $(0, 0, 0, 0), (1, 0, 0, 0)$ (no break of the $1 \rightarrow 2$ information flow)

Independent class: $(0, 1, 0, 0), (0, 0, 0, 1), (0, 1, 0, 1), \dots$ (any assignment that severs $1 \rightarrow 2$ or the measurement to 2)

In particular, the two assignments $(0, 1, 0, 0)$ (mechanistic outlier at X_2^*) and $(0, 0, 0, 1)$ (measurement outlier at X_2) are *observationally equivalent* with respect to the CI pattern between X_1 and X_2 : both induce independence of the observed pair and thus cannot be distinguished from pooled i.i.d. data using only CI tests on these two variables, whereas the assignments $(1, 0, 0, 0)$ and $(0, 0, 1, 0)$ can be distinguished. Similar phenomena occur in larger DAGs: assignments can still be observationally equivalent with respect to the observable CI patterns, but the number and composition of equivalence classes depend on the graph structure. Denser graphs tend to produce more diverse dependencies and thus smaller equivalence classes, whereas extremely sparse graphs yield larger equivalence classes where many assignments are indistinguishable.

A.2. Algorithmic Details

This section provides additional details on the proposed algorithm. Algorithm 1 in Sec. 4 illustrates the high-level procedure. Here, we elaborate on the key components: the fitting of the causal mechanisms, the estimation of the noise distributions, and the heuristic assignment and gain calculations.

One practical approximation is that we do not compute the full scores in Equation (3) for all samples and features. For samples that are unassigned and thus likely clean, we only compute the $O(1)$ mechanistic gains, avoiding the costly marginalization over all features for measurement gains. The rationale is that unassigned samples are expected to have low anomaly scores, so considering both outlier types provides minimal additional benefit.

A.2.1. CAUSAL MECHANISMS

To estimate the causal mechanisms, we use qgam (Fasiolo et al., 2021) with $q = 0.5$. We select the number of knots per parent as a simple rule of thumb:

$$m_{j,k} = \min \left\{ \max \left(5, \lfloor N^{1/3} / 2 \rfloor \right), 30 \right\}.$$

Knots are placed at empirical quantile breakpoints of the parent covariates, so that dense regions receive more knots (allowing flexibility) while sparse regions receive fewer (reducing variance).

A.2.2. MARGINALIZATION

Here, we provide further details on how to approximate the integral

$$\int \underbrace{\prod_{j \notin \mathcal{Z}_x} \hat{p}(x_j \mid \text{pa}_j)}_{\text{'clean' likelihood}} \underbrace{\prod_{j \in \mathcal{Z}_x} \tilde{p}_{O^{mech}_j}(x_j)}_{\text{mechanistic outlier density}} \underbrace{\prod_{j \in \mathcal{W}_x} dx_j}_{\text{latent clean values}}. \quad (5)$$

We approximate (5) via Monte Carlo integration over the latent clean values. Let $\mathbf{a} = (\mathbf{z}, \mathbf{w})$ be a fixed assignment and define $\mathcal{Z}_x = \{j : z_j = 1\}$ and $\mathcal{W}_x = \{j : w_j = 1\}$. For each $j \in \mathcal{W}_x$, let U_j denote the structural noise variable of

node j . Since we explicitly learn the distributions P_{U_j} , which capture the clean conditional noise, from the residuals of the causal mechanism fits, we can sample from these distributions. Latent clean values are obtained by sampling M times from the corresponding conditional distributions P_{U_j} for nodes in \mathcal{W}_x and propagating samples in topological order, and the resulting likelihoods are then averaged:

$$\int \underbrace{\prod_{j \notin \mathcal{Z}_x} \hat{p}(x_j \mid \text{pa}_j)}_{\text{'clean' likelihood}} \underbrace{\prod_{j \in \mathcal{Z}_x} \tilde{p}_{O^{\text{mech}}_j}(x_j)}_{\text{mechanistic outlier density}} \underbrace{\prod_{j \in \mathcal{W}_x} dx_j}_{\text{latent clean values}} \approx \frac{1}{M} \sum_{m=1}^M \underbrace{\prod_{j \notin \mathcal{Z}_x \cup \mathcal{W}_x} \hat{p}(x_j^{(m)} \mid \text{pa}_j^{(m)})}_{\text{'clean' likelihood}} \underbrace{\prod_{j \in \mathcal{Z}_x \setminus \mathcal{W}_x} \tilde{p}_{O^{\text{mech}}_j}(x_j^{(m)})}_{\text{mechanistic outlier density}},$$

$$x_j^{(m)} = \begin{cases} \hat{f}_j(\text{pa}_j^{(m)}) + \tilde{u}_j^{(m)}, & j \in \mathcal{W}_x \setminus \mathcal{Z}_x, \\ \tilde{o}_j^{(m)}, & j \in \mathcal{W}_x \cap \mathcal{Z}_x, \\ x_j, & j \notin \mathcal{W}_x, \end{cases} \quad \tilde{u}_j^{(m)} \sim P_{U_j}, \tilde{o}_j^{(m)} \sim P_{O_j^{\text{mech}}}.$$

By the law of large numbers, the Monte Carlo approximation converges to the true marginalization for $M \rightarrow \infty$.

A.2.3. HEURISTIC MLE ASSIGNMENT

The assignment procedure is summarized in Algorithm 2. The algorithm iteratively and greedily accepts candidate outlier assignments based on *optimistic gains*, which can be estimated without performing full marginalization. The procedure is decomposed into two main steps: assigning measurement outliers and then attributing residuals to mechanistic outliers.

Measurement outliers are first considered by sorting candidates according to their optimistic gains. Each candidate's gain is compared against the optimal alternative gain obtained from mechanistic attribution. Only candidates with positive optimistic gains that exceed the mechanistic alternative are accepted. The process continues until no remaining measurement candidates have positive optimistic gains.

For a measurement outlier candidate at node j and sample i , the optimistic gain $g_{i,j}^{\text{opt}}$ assumes that all affected residual likelihoods improve maximally, and then subtracts the cost of encoding the outlier and updating the Bernoulli probability. Specifically, the Bernoulli probability update can be approximated using the log of the binomial coefficient: encoding a sequence of k successes and $n - k$ failures with prefix codes based on empirical probabilities yields

$$-k \log \frac{k}{n} - (n - k) \log \frac{n - k}{n} \approx -\log \binom{n}{k},$$

i.e., the sequence-level Bernoulli code length is asymptotically equivalent to the binomial code length. For node j with $\sum_{i=1}^N W_j$ current measurement outliers, adding a new sample incurs a prior cost

$$-\log \hat{p}_{O_j^{\text{meas}}} + \left(-\log \left(\frac{N}{\sum_{i=1}^N W_j + 1} \right) + \log \left(\frac{N}{\sum_{i=1}^N W_j} \right) \right).$$

The full optimistic measurement gain is then

$$g_{i,j}^{\text{meas-opt}} = \sum_{k \in \{j\} \cup \text{Ch}(j)} \left[-\log \mathcal{L}(r_{ik}) - \min_r \{-\log \mathcal{L}(r)\} \right] + \log \hat{p}_{O_j^{\text{meas}}}(x_{i,j}) - \left[-\log \left(\frac{N}{\sum_{i=1}^N W_j + 1} \right) + \log \left(\frac{N}{\sum_{i=1}^N W_j} \right) \right],$$

where $\text{Ch}(j)$ denotes the children of node j , $\mathcal{L}(r_{ik})$ is the likelihood of the residual for node k and sample i , and $\hat{p}_{O_j^{\text{meas}}}$ is the current estimated prior of a measurement outlier at node j .

Intuitively,

1. The first term captures the maximal improvement in likelihood for affected nodes.

Algorithm 2 MLE-ASSIGN

Input: dataset D of size N , DAG \mathcal{G} , regressors $\{\hat{f}_k\}$, likelihoods $\{\mathcal{L}(R_k)\}$

Output: assignment $\mathbf{A} = (\mathbf{Z}, \mathbf{W})$

Notation: $g_{i,j}^{\text{meas-opt}}/g_{i,j}^{\text{mech-opt}}$ optimistic gains; $g_{i,j}^{\text{meas}}/g_{i,j}^{\text{mech}}$ actual gains

Initialization:

$\mathbf{A} \leftarrow (\mathbf{0}, \mathbf{0})$

Compute $g_{i,j}^{\text{opt}}$ for all (i, j)

$C \leftarrow \text{sorted}(\{(i, j)\}, g_{i,j}^{\text{meas-opt}})$ (descending)

Measurement pass:

for all $(i, j) \in C$ with $g_{i,j}^{\text{opt}} > 0$ **do**

 Compute $g_{i,j}^{\text{meas}}$

$g_{i,j}^{\text{comp}} \leftarrow \sum_{k \in \{j\} \cup \text{Ch}(j), g_{i,k}^{\text{mech}} > 0} g_{i,k}^{\text{mech}}$

if $g_{i,j}^{\text{meas}} > g_{i,j}^{\text{comp}}$ **then**

$\mathbf{W}[i, j] \leftarrow 1$

 Update $g_{i,\ell}^{\text{opt}}$ for affected (i, ℓ)

end if

end for

Mechanistic pass:

$C \leftarrow \text{sorted}(\{(i, j)\}, g_{i,j}^{\text{mech-opt}})$ (descending)

for all $(i, j) \in C$ **do**

if $\mathbf{W}[i, j] = 1$ **then**

continue

end if

 Compute $g_{i,j}^{\text{mech}}$

if $g_{i,j}^{\text{mech}} > 0$ **then**

$\mathbf{Z}[i, j] \leftarrow 1$

else

continue

end if

end for

return $\mathbf{A} = (\mathbf{Z}, \mathbf{W})$

2. The second term penalizes the prior probability of adding a new outlier.
3. The third term accounts for the combinatorial cost of updating the number of outliers.

Mechanistic gains are defined analogously, but depend only on the residual of the node itself, i.e.

$$\begin{aligned}
 g_{i,j}^{\text{mech-opt}} &= -\log \mathcal{L}(r_{ij}) - \min_r \{-\log \mathcal{L}(r)\} \\
 &\quad + \log \hat{p}_{O_j^{\text{mech}}}(x_{i,j}) \\
 &\quad - \left[-\log \left(\frac{N}{\sum_{i=1}^N Z_j + 1} \right) + \log \left(\frac{N}{\sum_{i=1}^N Z_j} \right) \right].
 \end{aligned}$$

If a node is not in the MB of a measurement outlier, this estimate is exact. Otherwise, exact gains are evaluated by calculating the likelihood after adding the outlier to the assignment, approximating marginalization as needed.

The overall procedure is as follows: MLE-ASSIGN performs the greedy measurement and mechanistic assignment passes. Candidates are processed in descending order of optimistic gain for measurements, and descending residual cost for mechanistic outliers. The final assignment $\mathbf{A} = (\mathbf{Z}, \mathbf{W})$ is then used to compute scores and classes.

A.2.4. COMPLEXITY.

Fitting one `qgam` per non-root node k has complexity $O(Nm_k^2)$, where m_k is the number of spline basis functions. With $m_k = O(N^{1/3}|\text{Pa}_j|)$, this gives $O(N^{5/3}d^2)$ in the worst case. Mechanistic gains are inexpensive, $O(1)$ per candidate. For measurement gains, we perform a constant number of model evaluations in the Markov-blanket space MB_j . Computing measurement gains for all features and samples thus gives $O(Nd^2)$. Our greedy procedure ensures, that we only compute a linear number of gains for each sample, avoiding the otherwise exponential search space. Overall, the worst-case complexity is

$$O\left(N^{5/3}d^2 + Nd^2\right) = O\left(N^{5/3}d^2\right).$$

This is pessimistic: typically, only a small subset of measurement candidates is considered, and parent sets / MBs are much smaller than d .

A.3. Implementation Details

In this section, we provide both the implementation details of all algorithms, we compared to, and the hyperparameter selection that we performed.

A.3.1. IMPLEMENTATION

CALI is implemented in Python, and uses the R package `qgam` (Fasiolo et al., 2021). Most of our competing detection methods, namely AE (Sakurada & Yairi, 2014), DEEPSVDD (Ruff et al., 2018), iFOREST (Liu et al., 2008), COPOD (Li et al., 2020), LOF (Breunig et al., 2000), are implemented with the Python library `pyod` (Zhao et al., 2019). We implemented the NF-based (Rezende & Mohamed, 2015) anomaly detection using the Python library `pzflow` (Crenshaw et al., 2024).

The competing RCA methods are combined with the best sample detector (aside from **CALI**) of the respective experiment. For the synthetic data, this is AE and for the real data NF. After applying the sample detectors, we threshold such that the highest $p\%$ of samples with the highest scores are removed from training, where p corresponds to the true percentage of anomalies.

For the calculation of Shapley values, we use the kernel explainer implemented in the `shap` library (Lundberg & Lee, 2017) with 100 background samples. For SMTR and SCOR, we use the published implementations. For DICE (Mothilal et al., 2020), and M2OE (Angiulli et al., 2024), we adapted the implementations published by the authors to our setting. We combined DICE with a thresholded autoencoder to simulate a classification problem.

As mentioned in the main paper, SCM* is an adaptation of existing SCM-based attribution approaches (Budhathoki et al., 2022; Strobl & Lasko, 2023a;b). The key distinction in our setting is that we aim to attribute anomalousness at the level of an entire sample, rather than the outlierness of an individual feature (Budhathoki et al., 2022) or a binary target (Strobl & Lasko, 2023a). In our formulation, sample anomalousness can be quantified with the joint density, which factorizes into independent noise distributions. Consequently, the conditional likelihoods already capture the individual feature contributions, making an explicit attribution step unnecessary. For the SCM, we use the exact same implementation as **CALI** to ensure a fair comparison.

A.3.2. HYPERPARAMETERS

Since all of our tasks are unsupervised, we tuned all hyperparameters, by selecting the ones with the best performance in our synthetic setup with different seeds than the data used for the actual evaluation.

CALI The only hyperparameter of **CALI** are the number of Monte Carlo samples, which we fixed to $K = 100$ across all experiments, and the KDE parameters. We fix the trimmed fraction $\alpha = 0.01$, and use a Gaussian kernel with bandwidth selected via Silverman's rule of thumb (Silverman, 2018) across all experiments.

Detection methods For competing detection methods, we conducted grid searches over: $bs \in \{32, 64, 128\}$, $e \in \{10, 100, 500\}$, $est \in \{100, 200, 300\}$, $neigh \in \{10, 20, 40\}$. The best configurations are summarized in Tab. 3.

Table 3. Best hyperparameters for detection methods.

Method	Batch size (bs)	Epochs (e)	Estimators (est)	Neighbors (neigh)
AE	32	10	–	–
NF	32	10	–	–
DEEPSVDD	128	100	–	–
iFOREST	–	–	300	–
LOF	–	–	–	10

RCA methods For the RCA methods, we searched over the same ranges of epochs and batch sizes. For M2OE, we additionally tuned the number of neighbors in the KNN step, $K \in \{10, 50, 100\}$, and for SMTR and SCOR we tested the anomaly detectors {MEDIANCDFQUANTILE, INVERSEDENSITY}. The selected configurations are shown in Tab. 4.

Table 4. Best hyperparameters for feature-level baselines.

Method	Batch size (bs)	Epochs (e)	KNN neighbors (K)	Detector
M2OE	32	500	100	–
SCOR	–	–	–	MEDIANCDFQUANTILE
SMTR	–	–	–	MEDIANCDFQUANTILE

MARG For MARG, we also compare two marginal outlier detectors based on estimated density and median distance, as well as significance levels $\alpha \in \{0.001, 0.01, 0.05, 0.1\}$ with and without Bonferroni correction. The best configuration uses the density-based detector with $\alpha = 0.01$ with Bonferroni correction.

A.4. Datasets

This section provides further detail about the synthetic and real-world datasets.

A.4.1. SYNTHETIC DATA

We generate synthetic observations $X \in \mathbb{R}^{N=2000 \times D=15}$ from a structural causal model (SCM) over a random DAG \mathcal{G} with 15 nodes. Each edge (i, j) , $i > j$, is included independently with probability $p_e = 0.3$, yielding an acyclic graph.

Clean variables follow

$$X_j^* = f_j(\text{Pa}_j) + U_j,$$

where $U_j \sim \mathcal{N}(0, \sigma^2)$ with $\sigma = 0.1$, and f_j is an additive polynomial mechanism normalized to $[0, 1]$ on the clean data.

Polynomial generation: Each function f_j is constructed as a sum of univariate polynomial components over its parent nodes. For a single parent input A , we generate a polynomial of length l as

$$f(A) = \sum_{i=1}^l a_i (A - b_i)^{e_i},$$

where

- a_i are random coefficients sampled uniformly from $[-1, -0.1] \cup [0.1, 1]$,
- b_i are random shifts sampled uniformly from $[-3, 3]$,
- $e_i \in \{2, 3\}$ are randomly chosen exponents.

For multivariate parents, the node function is the sum of the univariate polynomials applied independently to each parent:

$$f_j(\text{Pa}_j) = \sum_{k \in \text{Pa}_j} f_{jk}(X_k),$$

where each f_{jk} is generated as above. After evaluating the raw polynomials on the parent data, the outputs are normalized to $[0, 1]$ using min/max scaling to ensure numerical stability. We set $l = 2$ for all experiments.

Asymmetric outliers are introduced independently by sampling from the true distribution of X_j^* and shifting by k empirical standard deviations. For mechanistic outliers, downstream nodes are recalculated with resampled noise. This procedure is repeated across five seeds, and averages are reported.

We choose outlier ratios to obtain 10% sample contamination, with measurement and mechanistic outliers equally probable. Specifically,

$$\pi_j^{meas} = \pi_j^{mech} = 1 - (1 - 0.1)^{\frac{1}{2.15}} \approx 0.0035.$$

In every synthetic experiment, we average results over 20 random seeds, generating new graphs, mechanisms, and outlier injections each time.

A.4.2. SACHS DATASET

The Sachs dataset consists of simultaneous measurements of 11 phosphorylated proteins and phospholipids in human immune cells (Sachs et al., 2005). The data comprise both observational and interventional samples collected under multiple experimental conditions, and are commonly used as a benchmark for causal discovery. A consensus causal graph, derived from prior biological knowledge, is typically treated as ground truth. We present this graph in Fig. 7. Although the underlying biological signaling network may contain feedback loops, the benchmark graph used in most evaluations is represented as a directed acyclic graph (DAG). In our experiments, we follow this convention and remove the edge from $PIP3$ to $plcg$ to ensure acyclicity. The dataset contains 853 observational samples, and we introduce outliers as follows.

We simulate two types of outliers: (i) mechanistic, created by injecting a small fraction of interventional samples into the observational set, and (ii) measurement, created by selecting a column of an observational sample and replacing its value with the one of a value from a sample of the respective interventional distribution. For each variable, we introduce five mechanistic and five measurement outliers. We repeat this procedure across 20 random seeds.

A.4.3. CAUSAL CHAMBERS DATASET

In addition, we use the *Causal Chamber* benchmark (Gamella et al., 2025). It provides observational and interventional data from a controlled physical system with known ground-truth DAG. The graph is provided in Fig. 8. In each run we sample 2 000 observational samples and introduce outliers as follows.

As for the Sachs dataset, we simulate two types of outliers: (i) mechanistic, created by injecting a small fraction of interventional samples into the observational set, and (ii) measurement, created by selecting a column of an observational sample and replacing its value with the one of a value from a sample of the respective interventional distribution. Precisely, we randomly add $\frac{N}{20} \frac{0.05}{0.95} \approx 26$ random samples from each interventional dataset to contaminate approximately 5% of samples with mechanistic outliers. Additionally, we create the same amount of measurement outliers for each variable, by randomly selecting a column, and replacing it with the interventional column of an interventional sample. Again, we repeat this procedure across 20 random seeds.

The benchmark includes interventions labels as *mid* and *strong* for all variables but $L_{32}, L_{31}, L_{22}, L_{21}, L_{12}, L_{11}$. We evaluate the performance on the different strengths separately. Since the Sachs dataset contains much weaker interventions, we can separate the datasets by weak, medium and strong interventions. We provide the distribution of absolute z-scores of the interventional samples in Fig. 6.

A.4.4. NYC YELLOW TAXI TRIP DATASET

For the case study, we use the New York City Taxi & Limousine Commission (NYC TLC) Yellow Taxi trip dataset obtained from Kaggle (Elemento, n.d.). The analysis is restricted to data from January 2015 only. The dataset contains trip-level records for yellow taxis in New York City, including pickup and drop-off timestamps, trip distance, fare-related variables, passenger count, and geographic pickup and drop-off information recorded as coordinates. As an administrative dataset collected by the NYC TLC, it provides comprehensive coverage of yellow taxi activity during the study period. We preprocess the data by removing records with trivially missing or incorrect values such as zero coordinates, and select a random sample of size of 5 000 for our case study.

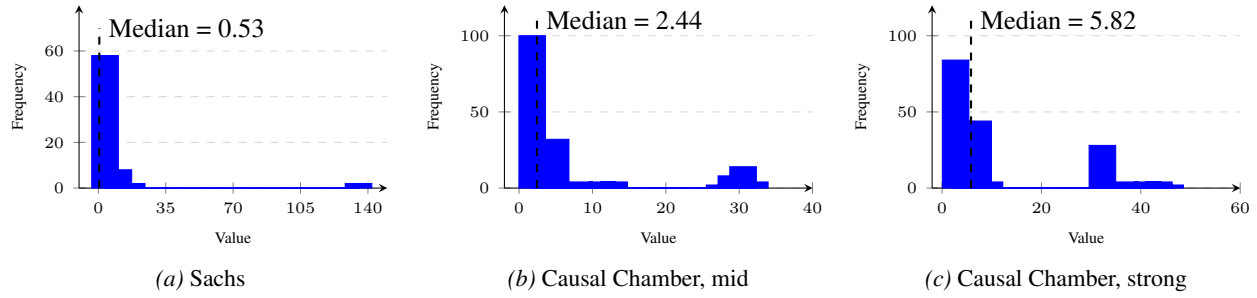


Figure 6. Distribution of absolute z-scores of interventional samples in the Sachs dataset (left), and Causal Chamber dataset with mid (center) and strong (right) interventions.

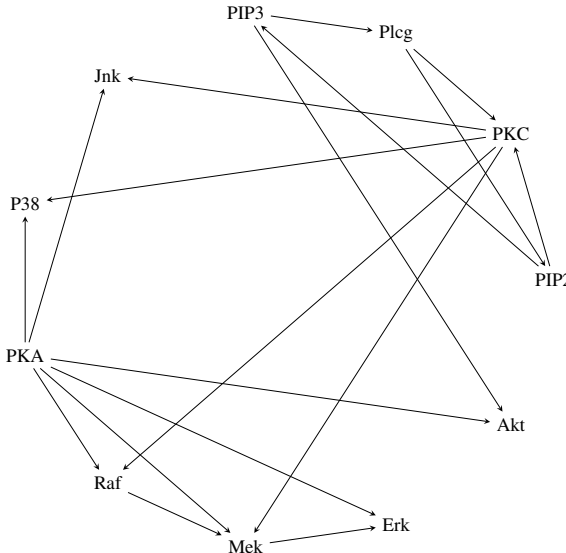


Figure 7. Consensus DAG of the Sachs dataset.

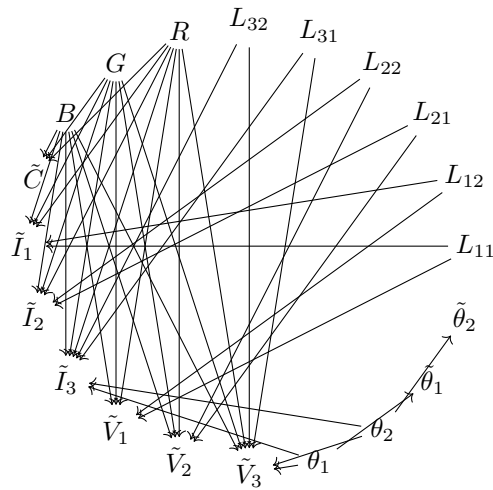


Figure 8. DAG of the light tunnel dataset of the *Causal Chamber* benchmark.

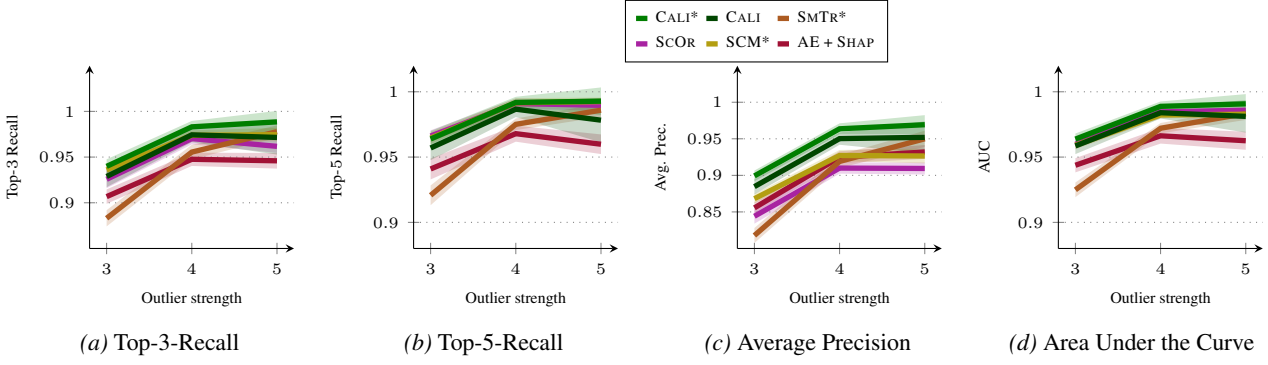


Figure 9. Additional metrics for root cause localization on synthetic data.

A.5. Additional Related Work

In addition, to the related work in the field of root cause analysis, we briefly discuss the broader field of outlier detection and explainable outlier detection.

Outlier Detection Outlier detection aims to identify observations that deviate from the bulk of the data. Traditional statistical methods, such as feature-wise Z-scores and Mahalanobis distance (Mahalanobis, 1936), are interpretable but limited in capturing complex dependencies. Machine learning-based approaches, including Local Outlier Factor (LOF) (Breunig et al., 2000), Isolation Forests (Liu et al., 2008), and One-Class SVM (Schölkopf et al., 2001), improve flexibility and robustness to structured deviations. Deep models, such as autoencoders (Sakurada & Yairi, 2014), normalizing flows (Rezende & Mohamed, 2015), and VAEs (Kingma & Welling, 2013), further capture highly nonlinear relationships at the cost of interpretability. For a comprehensive survey, see (Chandola et al., 2009; Pang et al., 2021).

Explainable Outlier Detection To improve interpretability, feature attribution methods like LIME (Ribeiro et al., 2016) and SHAP (Lundberg & Lee, 2017) have been adapted to anomaly scores (Friedman Antwarg et al., 2021), while counterfactual approaches (Wachter et al., 2017; Mothilal et al., 2020) identify minimal changes that would alter predictions. More recent methods (Angiulli et al., 2024) use masked transformation-based optimization to localize contributing features. For a survey on the field, see (Li et al., 2023). These methods provide feature-level explanations, but are largely correlation-based and rely on the learned structure of non-interpretable black-box models, which makes correct interpretation and classification of outlier types challenging.

A.6. Additional Experiments

In this section, we present a series of additional experiments designed to further evaluate and analyze our approach.

A.6.1. ADDITIONAL METRICS

In this section, we report additional evaluation metrics for the root cause localization experiments presented in the main paper.

We provide Top-3 Recall, Top-5 Recall, Average Precision (Avg. Prec.), and AUC in Fig. 9 and Fig. 10. Both Avg. Prec. and AUC are computed individually for each anomalous sample and then averaged across all anomalous samples.

A.6.2. RUNTIME

In Fig. 11 we present the runtime of CALI and its competitors. First, we fix the feature size to $d = 15$ and vary the sample size, then we fix the sample size to $N = 2000$, and vary the feature size. Notably, CALI is less efficient than competitors because of the combinatorial search over many features, and the causal discovery. If runtime is an issue, we recommend reducing the number of samples considered for the assignment. Currently, we assign all root causes that improve the global likelihood, which could be adjusted to only considering samples within top- k negative log likelihoods under the clean density.

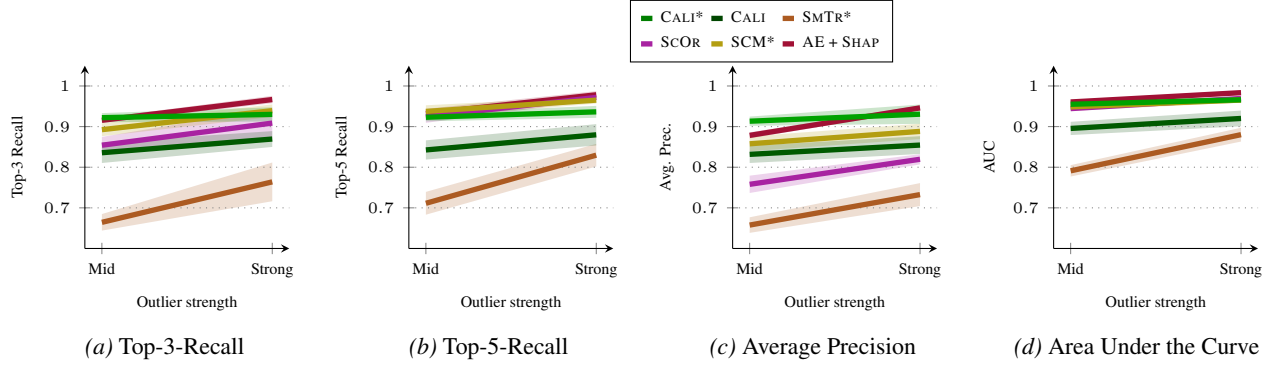


Figure 10. Additional metrics for root cause localization on the Causal Chamber dataset.

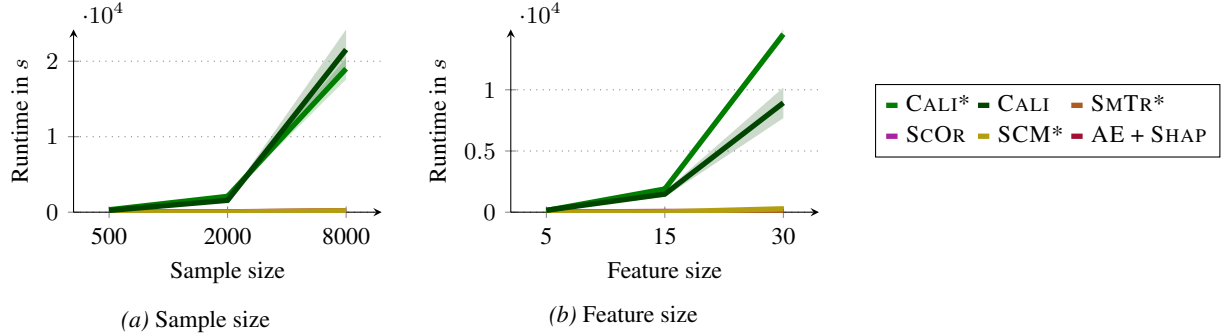


Figure 11. Runtimes for increasing sample and feature size.

A.6.3. ANOMALY DETECTION

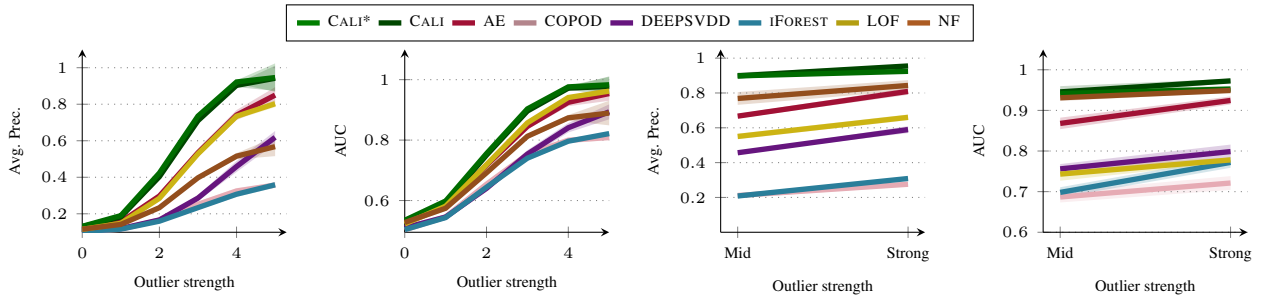
We compare against AE (Sakurada & Yairi, 2014), DEEPSVDD (Ruff et al., 2018), iFOREST (Liu et al., 2008), COPOD (Li et al., 2020), LOF (Breunig et al., 2000), and NF (Rezende & Mohamed, 2015).

We report AUC and Average Prevision (AP) for synthetic data and the Causal Chamber dataset (Fig. 12). Despite primarily being designed for characterization, CALI also performs great at detection.

A.6.4. ADDITIONAL RCA EXPERIMENTS

In this section, we provide various additional RCA experiments to further analyze the performance of CALI and its competitors.

Varying parameters in synthetic data generation. We repeat the synthetic experiment but vary either sample size, feature size, edge probability, or the expected number of root causes per expected sample. We use the same default settings as previously ($N = 2000$, $D = 15$, $p_e = 0.3$) and vary one of the factors. To analyze how the methods work under multiple


 Figure 12. Outlier Detection (\uparrow is better). Left: Synthetic data. Right: Causal Chamber dataset.

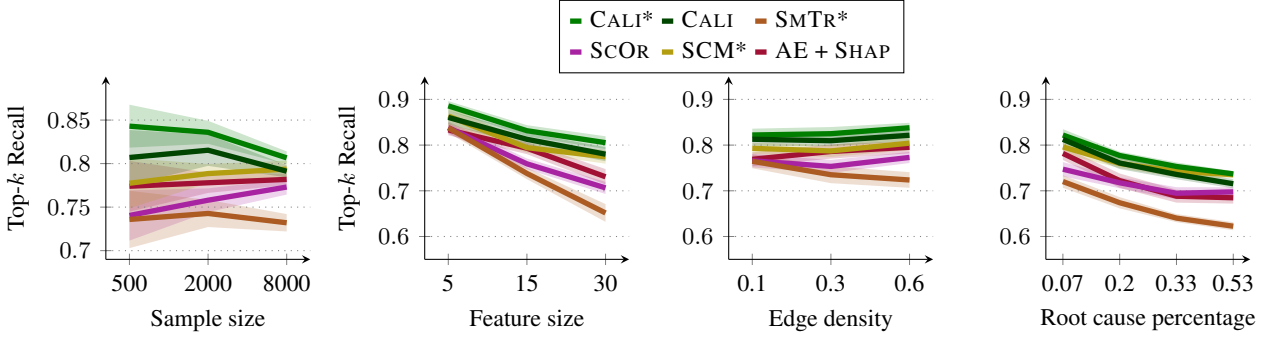


Figure 13. Root cause localization under varying parameters of the synthetic data generation.

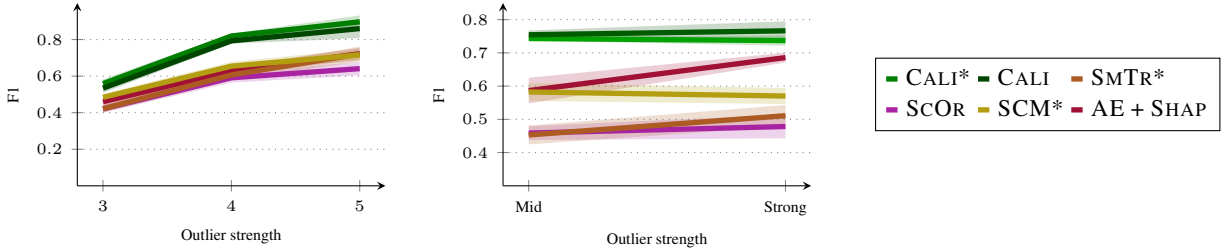


Figure 14. F1 scores of fixed assignments (\uparrow better). Left: Synthetic data, Right: Causal Chamber dataset.

root causes, we do one additional experiment we no longer use the independent Bernoulli draws, but instead randomly place rc_{count} root causes in 10% of samples, deciding with a coin flip whether we create a measurement or mechanistic outlier. We present the results in Fig. 13.

Individual outlier types We do an experiment under the default conditions, but only add one outlier type to evaluate how well the methods work for either type. We present the results in Fig. 15. While many methods work well when the data contains only measurement outliers, CALI*, SCM* and CALI perform best when it contains only mechanistic outliers.

Realistic RCA evaluation. To assess how many root causes can be realistically identified in practice, we conduct an additional experiment where we only evaluate RCA methods on samples that are actually detected as anomalous by a sample-level detector. This evaluation captures the practically relevant question of how many true root causes can be recovered when both anomaly detection and localization are imperfect, rather than assuming oracle knowledge of anomalous samples. We evaluate all competing RCA methods in combination with AE, which is the best-performing sample-level detector on the synthetic data, in order to obtain fixed binary predictions. Specifically, we first use the true sample contamination ratio to determine the corresponding score quantile of AE, yielding fixed anomaly predictions at the sample level. Next, for the samples predicted as anomalous, we apply the same procedure at the feature level using the RCA scores: we compute the ratio of root causes among truly anomalous samples and use it to select the corresponding quantile of the RCA scores. This process results in a binary prediction matrix indicating predicted root causes for each detected sample.

For CALI, this post-processing step is unnecessary, as the method directly outputs feature assignments through the learned model. We report Precision, Recall, and F1 score, with results shown in Fig. 14. On synthetic data, CALI* and CALI outperform all competing approaches by a large margin, achieving F1 scores of up to 0.8 for shifts of at least four standard deviations. This is particularly encouraging because, unlike competing methods, CALI does not rely on thresholding based on the true contamination ratio, which is typically unknown in practice. On the Causal Chamber dataset, CALI* and CALI likewise attain the best overall performance.

RCA for individual outlier types. Here we generate data with only one outlier type at a time to evaluate how well the methods can localize either mechanistic or measurement outliers. We use the same default settings as previously ($N = 2000, D = 15, p_e = 0.3$), and either only add measurement or mechanistic outliers. The results are presented in Fig. 15.

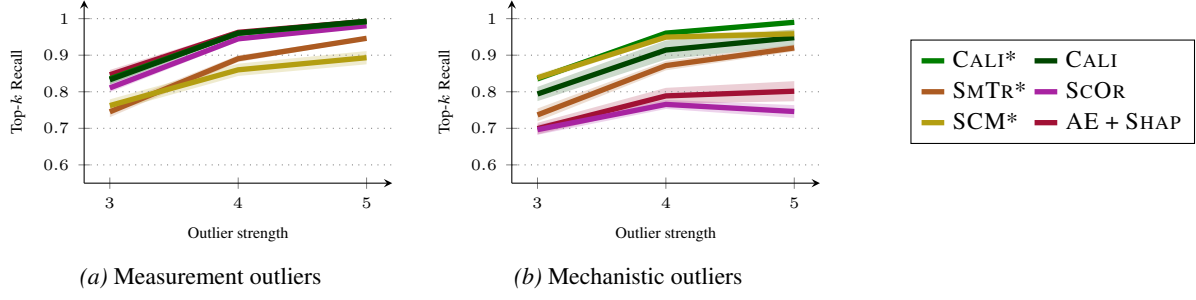


Figure 15. Root cause localization for the individual outlier types.

Table 5. Root cause localization and classification on the Sachs dataset. The highest performance is bolded.

Metric \ Method	AE-REC	AE-SHAP	MARG*	MARG	CALI	CALI*	SCM*	SCOR	SMTR
Top-3 Recall	0.412 ± 0.050	0.435 ± 0.041			0.438 ± 0.057	0.402 ± 0.042	0.412 ± 0.049	0.414 ± 0.043	0.347 ± 0.036
Top-5 Recall	0.548 ± 0.052	0.573 ± 0.039			0.620 ± 0.075	0.587 ± 0.068	0.544 ± 0.054	0.550 ± 0.041	0.564 ± 0.048
Top- k Recall	0.269 ± 0.026	0.279 ± 0.046			0.236 ± 0.036	0.192 ± 0.036	0.236 ± 0.036	0.240 ± 0.032	0.187 ± 0.032
Avg. Prec.	0.416 ± 0.027	0.430 ± 0.034			0.410 ± 0.034	0.375 ± 0.032	0.399 ± 0.030	0.376 ± 0.027	0.337 ± 0.024
AUC	0.586 ± 0.039	0.606 ± 0.032			0.623 ± 0.042	0.604 ± 0.043	0.591 ± 0.028	0.584 ± 0.033	0.558 ± 0.024
Accuracy					0.663 ± 0.077	0.847 ± 0.075	0.898 ± 0.097	0.860 ± 0.090	

A.6.5. SACHS DATASET

The full results of the Sachs experiment are reported in Table 5. Clearly, the dataset is quite challenging, as all methods achieve much lower RCA performance compared to the synthetic data or the Causal Chamber dataset. Somewhat surprisingly, CALI outperforms CALI* on most root-cause localization metrics, while MARG and CALI achieve the best overall classification performance. Notably, for the root causes that can be detected, the classification accuracy of 84% is even better than for the synthetic data. We attribute the fact that CALI outperforms CALI* to the factor that the data may not be entirely faithful to the assumed ground-truth DAG. Since it is known that the system contains feedback loops, the agreed-upon DAG is only an approximation. The fact that MARG* performs significantly worse than MARG further supports

A.6.6. CLASSIFICATION EXPERIMENTS

In this section we provide additional experiments related to the classification of outlier types.

CALI and MARG variants In Fig. 16, we compare the classification performance of CALI and MARG with a learned causal DAG. The experimental conditions are identical to the main paper. Surprisingly, the performance on the Sachs dataset is much better than on Causal Chamber despite weaker interventions, possibly because the learned DAG is more accurate. Overall, CALI outperforms MARG on synthetic data, whereas no method is consistently better on the real data. Since this is very different from the results with the ground-truth DAG, we attribute this to the learned DAG restricting classifications to trivial cases, which MARG can handle well.

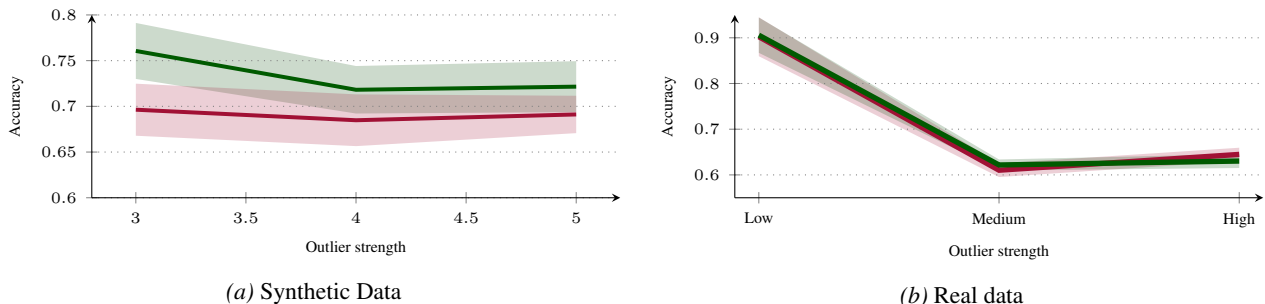


Figure 16. Classification performance of CALI and MARG with learned causal DAG.

Sample classification Instead of inspecting classification performance at the level of detected root causes, as done in the main paper, we also consider classification at the sample level. In our causal setting, each sample may contain measurement failure(s), mechanistic failure(s), or both. However, the presence of unidentifiable sink nodes complicates a direct sample-level categorization, as failures at such nodes cannot be causally distinguished without additional assumptions. Representing all possible combinations would therefore require introducing several additional and potentially unintuitive classes.

LaRosa et al. (2022) propose a classification method for a related but simpler problem. Their approach distinguishes between *sensor anomalies*, defined as failures affecting exactly one observed feature, and *process anomalies*, defined as failures affecting multiple features, in addition to the *normal* class. Under this definition, mechanistic failures at sink nodes are interpreted as sensor anomalies, and multiple independent mechanistic failures are classified as process anomalies. Consequently, their method does not aim to identify causal failure mechanisms in the data-generating process, but rather distinguishes whether none, exactly one, or more than one marginal distribution of the observed variables has changed.

Nevertheless, we compare CALI with the approach of LaRosa et al. under their classification scheme to assess whether incorporating causal structure also improves performance on this simpler sample-level task. Sample-level predictions for CALI are obtained by aggregating the inferred root-cause assignments. Specifically, whenever CALI assigns a mechanistic root cause to a node with successors, or assigns multiple root causes, we classify the sample as a *process anomaly*. When exactly one root cause is assigned and it corresponds either to a measurement failure or to a failure at a sink node, we classify the sample as a *sensor anomaly*. Samples without any assigned root cause are classified as *normal*.

The method of LaRosa et al. is originally designed for time-series data and is therefore adapted to the tabular setting. First, we separate the data into clean and anomalous samples using an autoencoder. Next, we generate 100 random groups of features of size three. These groups serve as inputs to gradient boosting prediction models, one for each feature, resulting in a total of $100 \times D$ predictors (1,500 predictors for $D = 15$). Classification is performed by thresholding the residuals of these predictors into normal and abnormal; we evaluate multiple significance levels $\alpha \in \{0.001, 0.01, 0.05, 0.1\}$.

Based on these binary residual predictions, LaRosa et al. define the following classification rule: if no residual is classified as abnormal, the sample is labeled *normal*. If there exists a feature i for which all corresponding groups predict abnormal residuals, and no other feature j (predicted from any group not containing i) is classified as abnormal, the sample is labeled *sensor anomaly*. In all remaining cases, the sample is classified as *process anomaly*.

We present the results in Figure 17.

Influence of degree To analyze classification behavior under different structural conditions, we begin with a three-variable chain $X_1 \rightarrow X_2 \rightarrow X_3$ and introduce both a measurement and a mechanistic outlier at X_2 . We then progressively add parent and child nodes to X_2 and evaluate how classification accuracy changes. For each graph structure, we generate random nonlinear functions and noise following the setup of the previous synthetic experiments. Classification accuracy is averaged over 50 runs, counting only those runs in which both root causes are correctly identified. Fig. 18 summarizes the results.

Surprisingly, MARG* outperforms CALI* when X_2 has two parents and two children; however, its performance degrades once an additional parent and child are added. This is probably because the optimal significance threshold to determine marginal outlierness depends on the degree. This suggests that if the outliers are strong enough that propagation can easily be detected, we need the right threshold, which is impossible to choose in the unsupervised setting. In contrast, the performance of CALI* improves consistently as the degree of the outlier node increases, without requiring the selection of a significance threshold.

Confidence Last but not least, we look at the confidence scores produced by CALI. Specifically, we evaluate how well the confidence scores rank correct classifications, by evaluating the AUC and calculating the Spearman correlation. We present the results in Fig. 19.

A.6.7. CAUSAL DISCOVERY

In this experiment, we evaluate the performance of CALI on DAGs learned using different causal discovery algorithms, namely TOPIC (Xu et al., 2025), CAM (Bühlmann et al., 2014), SCORE (Rolland et al., 2022), NoGAM (Montagna et al., 2023), and NOTEARS-MLP (Zheng et al., 2020). We run the algorithms under three different settings on our synthetic data.

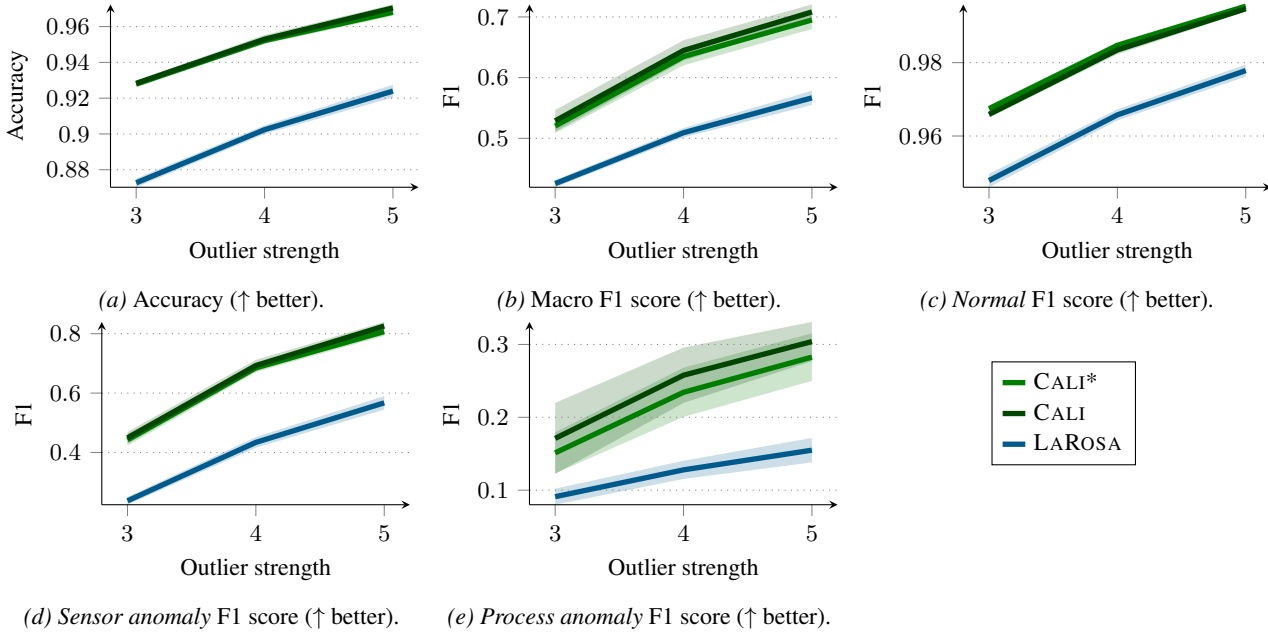


Figure 17. Classification into the classes *Normal*, *Sensor Anomaly*, *Process Anomaly*. Accuracy, macro F1, and per-class F1 scores are reported due to class imbalance.

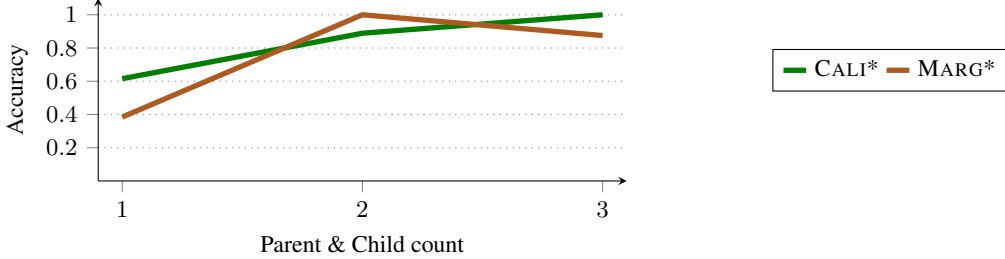


Figure 18. Influence of node degree on classification accuracy.

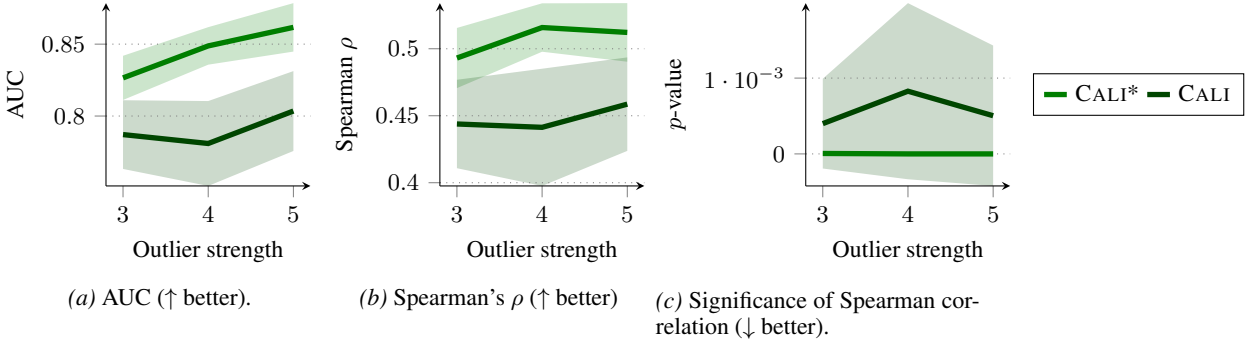


Figure 19. We evaluate the confidence scores of CALI by evaluating the ranking of true positive predictions, in terms of AUC and Spearman correlation. Overall the confidence scores produce a clear but imperfect signal, which is likely due to their heuristic nature. The confidence scores are weakly positively correlated with true positive predictions, and clearly significant at $\alpha = 0.05$.

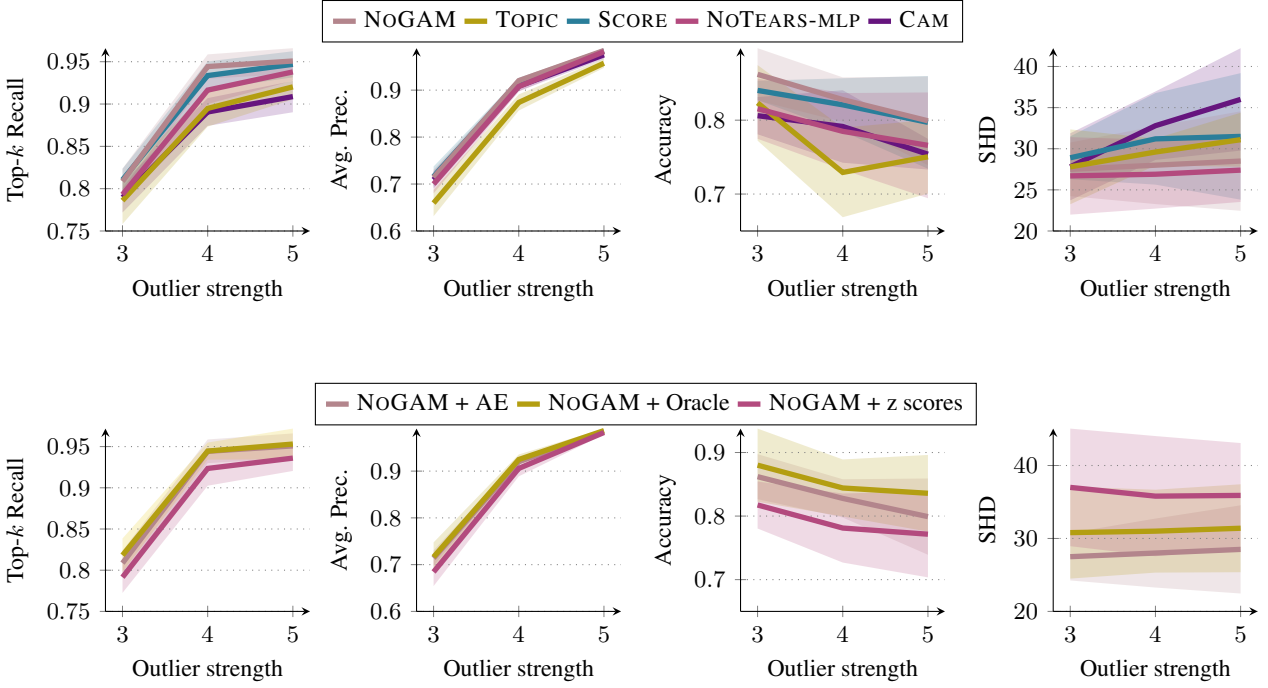


Figure 20. Performance of CALI when combined with different causal discover algorithms. Top- k Recall, and Avg. Prec. assess the downstream root cause localization, Accuracy assess outlier type classification and Structural Hemming Distance (SHD) similarity to the true DAG. Top: Different algorithms with AE prefiltering. Bottom: NOGAM with different prefiltering strategies.

First, they have access to the clean data. Second, we apply filtering to the corrupted data using either an autoencoder or robust z-scores based on the median and MAD. In both cases, we remove values within the 0.95 quantile and then learn the DAG from the filtered data. Overall the AE prefiltering performs better than z-scores, and NOGAM achieves the best downstream performance. We report all methods with AE prefiltering, and the different prefiltering strategies with NOGAM in Fig. 20.

A.6.8. NON-CAUSAL RCA

For non-causal RCA methods without a notion of causal structure, we evaluate AE-SHAP, AE-REC, M2OE (Angiulli et al., 2024), and DICE (Mothilal et al., 2020). We present the results in Fig. 21. AE-SHAP performs best with M2OE coming in second. DICE clearly shows the worst performance. We want to emphasize that none of these methods are designed for the task that we evaluate them on, and we include them here for completeness. Our main experiments indicate that AE-SHAP still performs surprisingly well, even without access to the causal structure or causal guarantees.

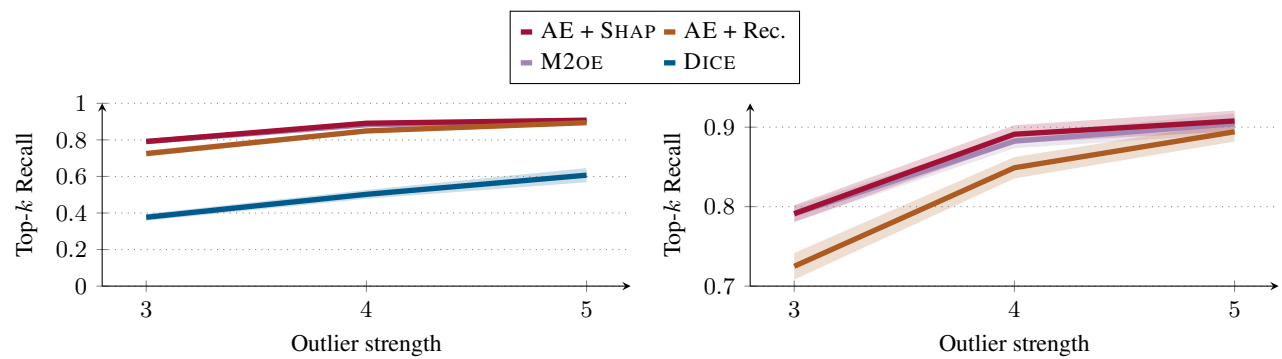


Figure 21. Root cause localization (\uparrow better) on synthetic data.